Tropical Cooling at the Last Glacial Maximum: An Atmosphere–Mixed Layer Ocean Model Simulation

ANTHONY J. BROCCOLI

NOAA/Geophysical Fluid Dynamics Laboratory, Princeton University, Princeton, New Jersey

(Manuscript received 20 November 1998, in final form 10 May 1999)

ABSTRACT

The sensitivity of tropical temperature to glacial forcing is examined by using an atmosphere–mixed layer ocean (A–MLO) model to simulate the climate of the last glacial maximum (LGM) following specifications established by the Paleoclimate Modeling Intercomparison Project. Changes in continental ice, orbital parameters, atmospheric CO_2, and sea level constitute a global mean radiative forcing of -4.20 W m^{-2}, with the vast majority of this forcing coming, in nearly equal portions, from the changes in continental ice and CO_2. In response to this forcing, the global mean surface air temperature decreases by 4.0 K, with the largest cooling in the extratropical Northern Hemisphere. In the Tropics, a more modest cooling of 2.0 K (averaged from 30°N to 30°S) is simulated, but with considerable spatial variability resulting from the interhemispheric asymmetry in radiative forcing, contrast between oceanic and continental response, advective effects, and changes in soil moisture. Analysis of the tropical energy balance reveals that the decrease in top-of-atmosphere longwave emission associated with the tropical cooling is balanced primarily by the combination of increased reflection of shortwave radiation by clouds and increased atmospheric heat transport to the extratropics.

Comparisons with a variety of paleodata indicate that the overall tropical cooling is comparable to paleoceanographic reconstructions based on alkenones and species abundances of planktonic microorganisms, but smaller than the cooling inferred from noble gases in aquifers, pollen, snow line depression, and the isotopic composition of corals. The differences in the magnitude of tropical cooling reconstructed from the different proxies preclude a definitive evaluation of the realism of the tropical sensitivity of the model. Nonetheless, the comparisons with paleodata suggest that it is unlikely that the A–MLO model exaggerates the actual climate sensitivity. The similarity between the sensitivity coefficients (i.e., the ratio of the change in global mean surface air temperature to the change in global mean radiative forcing) for the LGM simulation and a simulation of CO_2 doubling suggests that similar climate feedbacks are involved in the responses to these two perturbations. More comprehensive simulation of the tropical temperature sensitivity to glacial forcing will require the use of coupled models, for which a number of technical obstacles remain.

1. Introduction

The magnitude of tropical cooling during the last ice age remains an unresolved issue in paleoclimatology. The first quantitative estimates of tropical temperature change on a global scale came from the Climate: Long-Range Investigation Mapping and Prediction (CLIMAP) project and were based on the abundances of planktonic microfossils in deep-sea sediment cores. Preliminary reconstructions of August sea surface temperature (SST) from this project indicated a low-latitude cooling averaging approximately 2 K (CLIMAP Project Members 1976). Webster and Streten (1978) noted that a cooling of this magnitude was in potential conflict with the 6–8-K glacial cooling for the New Guinea mountains estimated from geological evidence of lower snow lines. They concluded that it was highly unlikely that these two temperature estimates could be reconciled.

Further analysis by CLIMAP led to more comprehensive SST reconstructions for both August and February utilizing data from additional sediment cores (CLIMAP Project Members 1981). Low-latitude cooling was even smaller than indicated in the original CLIMAP reconstruction, with average temperature changes of perhaps 1 K in the deep Tropics. Substantial areas in the subtropics were depicted as having higher temperatures during glacial times. Rind and Peteet (1985) questioned the low-latitude temperatures in this reconstruction. They found that a climate model forced at its lower boundary with the CLIMAP SST reconstruction produced atmospheric temperatures warmer than those estimated from a variety of snow line depression and pollen data.

The recent development of new methods of paleotemperature estimation have not satisfactorily resolved this issue. Broecker (1995) provides an excellent sum-

Corresponding author address: Dr. Anthony J. Broccoli, NOAA/GFDL, Princeton University, P.O. Box 308, Forrestal Campus, U.S. Route 1, Princeton, NJ 08542.
E-mail: ajb@gfdl.gov

mary of these methods and the results they have produced. Temperature reconstructions based on noble gases in aquifers and isotopic analysis of corals indicate low-latitude glacial temperatures approximately 5 K cooler than today, generally consistent with the pollen and snow line evidence. On the other hand, analysis of the temperature-dependent production of alkenone molecules by marine organisms yields smaller temperature changes averaging about 2 K, or closer to the CLIMAP estimates. Utilization of these new techniques for paleotemperature reconstruction is in a relatively early stage, so sites are few and global coverage is not yet possible. Nevertheless, those estimates that are available still allow considerable uncertainty about the magnitude of low-latitude glacial cooling.

Uncertainty regarding tropical temperature changes at the last glacial maximum (LGM) has significance beyond paleoenvironmental reconstruction. The question of how the Tropics respond to changes in climate forcing has become an important issue in climate dynamics. Pre-Pleistocene paleoclimatic evidence is generally interpreted to indicate only small variations in tropical temperatures as compared to those at high latitudes (Crowley 1991), which would support the hypothesis that tropical temperatures may be relatively insensitive to changes in radiative forcing. This has important implications for future climate change, given that climate models simulate sizeable changes in low-latitude temperature in response to imposed changes in atmospheric greenhouse gas concentration.

In attempts to simulate the LGM climate, coupled atmosphere–mixed layer ocean (A–MLO) models have simulated significant tropical cooling (e.g., Manabe and Broccoli 1985b). Much of the cooling at those latitudes occurs in response to the reduced CO_2 content of the glacial atmosphere (Broccoli and Manabe 1987), which is imposed based on chemical analyses of air bubbles in ice cores (e.g. Barnola et al. 1987). Thus the magnitude of tropical temperature change during the last ice age may be an important benchmark for evaluating whether current climate models respond realistically to radiative forcing such as that produced by greenhouse gases, despite the uncertainty inherent in the paleoclimatic estimates.

For this reason, we will examine the response of an atmosphere–mixed layer ocean model to the imposition of climate forcing from the LGM. The particular emphasis of this paper will be on simulated changes in temperature in and near the Tropics, and some of the mechanisms influencing the spatial distribution of temperature response. Simulated changes in temperature will be compared with a variety of paleodata derived from different methods, and the implications for climate model sensitivity will be discussed.

2. Model description

The climate model used in this study consists of three primary components: 1) a general circulation model of the atmosphere, 2) a heat and water balance model over the continents, and 3) a simple mixed layer ocean model that includes sea ice. Although the individual components have undergone modification, the procedure for coupling these components essentially follows that of Manabe and Stouffer (1980), except for the addition of a heat flux adjustment that will be described later in this section.

The dynamical component of the atmospheric model was developed by Gordon and Stern (1982), and is very similar to that developed by Bourke (1972). It employs the spectral transform method, in which the horizontal distributions of the primary variables are represented by spherical harmonics. The present model retains 30 zonal waves, adopting the so-called rhomboidal truncation. The spacing of the corresponding transform grid is 2.25° lat $\times$ 3.75° long. Normalized pressure (σ) is used as the model's vertical coordinate, with 20 unevenly spaced levels used for finite differencing. An additional characteristic of the model is a parameterization of the drag that results from the breaking of orographically induced gravity waves. A description of this parameterization and a discussion of its impact on the simulation of climate are contained in Broccoli and Manabe (1992).

Solar radiation at the top of the atmosphere is prescribed, varying seasonally but not diurnally. Computation of the flux of solar radiation is performed using a method similar to that of Lacis and Hansen (1974), except that the bulk optical properties of various cloud types are specified. Terrestrial radiation is computed as described by Stone and Manabe (1968). For the computation of radiative transfer, clouds are predicted using a relative humidity–dependent scheme similar to that of Wetherald (1996), except that the critical relative humidity values for the top of the atmosphere and the surface are 96% and 100%, respectively. The mixing ratio of carbon dioxide is assumed constant everywhere, and that of ozone is specified as a function of height, latitude, and season.

In the continental submodel, surface temperatures are computed from a heat balance with the requirement that no heat is stored in the soil. Both snow cover and soil moisture are predicted. A change in snow depth is predicted as the net contribution from snowfall, sublimation, and snowmelt, with the latter two quantities determined from the surface heat budget. Soil moisture is computed by the ''bucket method.'' The soil is assumed to have a water-holding capacity of 15 cm. If the computed soil moisture exceeds this amount, the excess is assumed to be runoff. Changes in soil moisture are computed from the rates of rainfall, evaporation, snowmelt, and runoff. Evaporation from the soil is determined as a function of soil moisture and the potential evaporation rate (i.e., the hypothetical evaporation rate from a completely wet soil). Further details of the hydrologic computations can be found in Manabe (1969).

The oceanic component of the model treats the ocean mixed layer as a vertically isothermal layer of static

water with a uniform thickness of 50 m. A heat flux adjustment, which varies with location and season, is added at each grid point to compensate for the absence of horizontal heat transport by representing the convergence or divergence of heat by ocean currents (Hansen et al. 1984; Wilson and Mitchell 1987). If the temperature of the mixed layer ocean decreases to its freezing point, any additional heat loss results in sea ice formation. Sea ice dynamics and thermodynamics are simulated by an adaptation of the cavitating fluid model of Flato and Hibler (1992).

Thus there have been a number of model improvements relative to the previous ice age simulation experiments described by Manabe and Broccoli (1985b), Broccoli and Manabe (1987), and Broccoli and Marciniak (1996). The model resolution has been increased in both the horizontal (from R15 to R30) and vertical (from 9 to 20 levels). This increase in resolution produces improvements in several aspects of the simulation of modern climate, including the circumpolar trough around Antarctica, the Northern Hemisphere wintertime stationary waves, the dry climates of the Eurasian interior, and the sharpness of the intertropical convergence zone. The use of a heat flux adjustment to mimic the thermal effects of ocean circulation yields a better simulation of the sea ice margin, a quality that is essential for the realistic simulation of sea ice–albedo feedback. Also, the incorporation of sea ice dynamics should produce a more realistic representation of air–sea heat flux in sea ice–covered areas, since the cavitating fluid sea ice model allows for the formation of leads.

3. Experimental design

To investigate the climate of the ice age Tropics, a simulation of the LGM climate is produced by integrating the model described in the previous section and comparing it to a simulation of the modern climate using the same model. In order to simulate the LGM climate, a number of model inputs (i.e., ''boundary conditions'') are altered from their modern values. These include the orbital parameters of the earth, sea level, land–sea distribution, continental ice distribution, surface elevation, and atmospheric CO_2 concentration. This experimental design corresponds to the specifications established by the Paleoclimate Model Intercomparison Project (PMIP), an international initiative devoted to comparing the results of LGM and mid-Holocene simulations from a large number of climate models (Joussaume and Taylor 1995).

In obtaining the earth's orbital parameters, the timescale of Bard et al. (1990) is adopted, which places the LGM at 21 kyr BP. Orbital parameters for 21 kyr BP are taken from the work of Berger (1978). The sea level reduction of 105 m and the three-dimensional ice sheet distribution are taken from the geophysical inverse calculation of Peltier (1994), which also determines the land–sea distribution and surface elevation. In both the modern and LGM simulations, the method of Lindberg and Broccoli (1996) is used to convert gridded surface elevations into smooth spectral topography. The atmospheric CO_2 content for the LGM simulation is reduced by approximately 25% to represent the glacial-to-preindustrial difference in CO_2 based on the analysis of air bubbles in ice cores (e.g., Barnola et al. 1987).

To conform with the PMIP specifications, several other possible changes in LGM climate forcing were not included. Despite a variety of evidence suggesting increased atmospheric dust loading during the glacial, no attempt was made to alter the dust content of the model atmosphere, because of uncertainties in the spatial distribution and optical properties of dust. Neither were there any vegetation-induced changes in the surface albedo of snow-free land, because of uncertainties in the distribution of LGM vegetation. Finally, there was no attempt to represent the glacial decrease in methane and nitrous oxide determined from ice cores; based on the expressions compiled by Shine et al. (1990), the reduction of infrared trapping resulting from the decreased concentrations of these gases would add approximately 16% to the overall radiative forcing of the LGM integration.

The changes in land–sea distribution and surface elevation introduce some complications in the experimental design. The reduction of sea level in the LGM integration exposes additional land points that are not present in the modern integration and, thus, do not have base (i.e., snow free) albedos determined from observations. Where these points are covered by continental ice, they are assigned surface albedo values accordingly. In those locations where such points are ice free, they are assigned a base albedo determined from the nearest neighboring points.

Another difficulty brought about by the change in land–sea distribution involves the heat flux adjustment. As discussed earlier, this flux is added at each grid point to mimic the convergence of heat due to transport by ocean currents. For the LGM integration, some change in the distribution of the heat flux adjustment is necessitated by the change in continental area. An arbitrary decision was made to redistribute the adjustment from emerged land points uniformly among the remaining ocean points at that latitude. This has the effect of preserving the implied heat transport by the ocean across latitude circles.

Finally, the gravity wave drag parameterization requires the spatial distribution of topographic variance on scales smaller than a model grid box (Broccoli and Manabe 1992). Because the surface elevation reconstruction is not of sufficient spatial detail to compute this quantity, the distribution of subgrid-scale variance based on the modern topography is used in the LGM integration. This will introduce some error over the regions covered by LGM continental ice, but little or no error over the much larger ice-free areas.

The initial condition for the modern integration was

TABLE 1. Annually averaged net radiative forcing (W m^{-2}) of LGM integration by forcing mechanism and geographical region.

	Global	Northern Hemisphere	Southern Hemisphere	Tropics (30°N–30°S)	Northern Hemisphere Tropics (0°–30°N)	Southern Hemisphere Tropics (0°–30°S)
Continental ice	−1.88	−3.46	−0.31	0.00	0.00	0.00
Atmospheric CO_2	−1.99	−1.99	−1.99	−2.15	−2.13	−2.18
Orbital parameters	+0.04	+0.02	+0.07	+0.49	+0.52	+0.46
Sea level change	−0.37	−0.49	−0.26	−0.55	−0.75	−0.35
Combined effect	−4.20	−5.92	−2.49	−2.21	−2.35	−2.07

taken from an integration in which the SST and sea ice distributions were prescribed, varying seasonally, based on climatological observations. The model was then allowed to determine its own SST and sea ice distribution, after which it was integrated for 20 yr to settle into a quasi-equilibrium climate. An additional 25 yr beyond this adjustment period were archived for further analysis. A similar procedure was employed for the LGM integration, with an initial condition chosen from the modern integration and the LGM forcing applied. Fifty years of integration were required for the model to adjust to this substantial change in forcing, and the 20 yr following this adjustment period were archived.

Two other A–MLO model integrations are briefly discussed in this paper. The LGM-NE integration incorporates all of the forcings included in the LGM integration except that the surface elevation is exactly the same as the modern integration. Thus the expanded continental ice sheets are represented by a permanent, infinitesimally thin ice layer superimposed on the modern topography. The $2 \times CO_2$ integration is identical to the modern integration except that the atmospheric CO_2 concentration is doubled. The initial condition for each of these integrations was chosen randomly from the modern integration, and the model was integrated through a 40-yr spinup period. Subsequently, output from the LGM-NE and $2 \times CO_2$ integrations was archived for 10 and 20 yr, respectively, for further analysis. Unless otherwise stated, the time averages for each of these integrations are based on the entire period of archived output.

4. Radiative forcing

The alteration of the orbital parameters, sea level, land–sea distribution, continental ice distribution, surface elevation, and atmospheric CO_2 concentration to values representative of the LGM constitutes a radiative forcing of the climate system. Both the large continental ice sheets and the expanded land area (due to lowered sea level) result in a negative net forcing by increasing the surface albedo. The reduction of CO_2 also constitutes a negative net forcing by decreasing the opacity of the atmosphere to infrared radiation. Changes in orbital parameters alter the seasonal and spatial distribution of solar radiation at the top of the atmosphere and, thus, produce a forcing that varies spatially in sign.

To quantify the radiative forcing, a series of calculations was made using the radiative transfer component of the climate model. In each calculation, one or more of the above changes was imposed while maintaining the surface and atmospheric quantities (e.g., temperature, water vapor mixing ratio, clouds) at values taken from the modern integration. The resulting change in net irradiance at the tropopause is the instantaneous radiative forcing as defined by Shine et al. (1994). To integrate the instantaneous radiative forcing over the entire seasonal cycle, the radiation-only calculations were performed once per day for a year, using three-dimensional distributions of temperature, water vapor mixing ratio, and clouds sampled daily from the modern integration.

Results from radiative forcing calculations are displayed in Table 1. On a global basis, the large continental ice sheets over North America and Eurasia are responsible for nearly half of the radiative forcing of the LGM integration (-1.88 W m^{-2}), as these ice sheets reflect a very large fraction of incoming solar radiation. The reduction of atmospheric CO_2 is the other major source of radiative forcing. By decreasing the infrared opacity of the atmosphere, it leads to a global average forcing of -1.99 W m^{-2}. The effects of expanded continental ice and reduced CO_2 combine to account for more than 90% of the overall radiative forcing. The lower sea level at the LGM also contributes a modest negative forcing (-0.37 W m^{-2}), because the albedos specified for land points are generally higher than those specified for sea points. Differences in the geometry of the earth's orbit produce very little globally averaged forcing ($+0.04$ W m^{-2}).

Although the effects of expanded continental ice and decreased CO_2 contribute almost equally to the global radiative forcing, their spatial distributions are very different. Most of the ice sheet forcing occurs in the zonal belt from 40° to 80°N (Fig. 1), with a smaller region of ice sheet forcing in the zonal belt from 60° to 80°S, where the Antarctic ice sheet expanded across the continental shelf at the LGM. Sea level lowering is responsible for an irregular pattern of zonal mean forcing (generally <1 W m^{-2}) at low latitudes. In contrast to the nonuniform pattern of surface albedo forcing, the CO_2 forcing is much more homogeneous and is almost perfectly symmetric between the two hemispheres. The

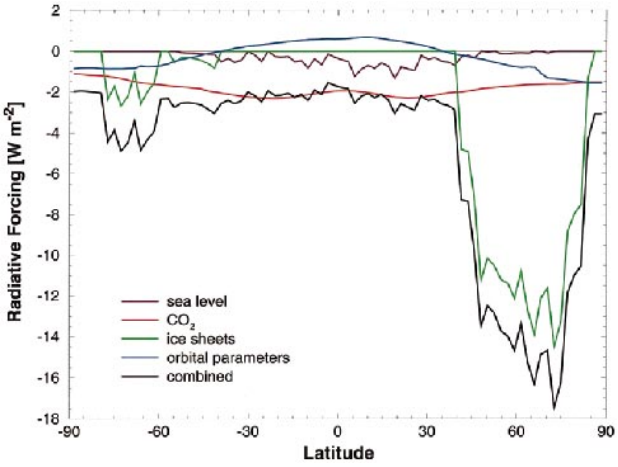

FIG. 1. Zonally averaged annual mean radiative forcing of LGM integration from sea level reduction (purple), atmospheric CO_2 (red), continental ice sheets (green), orbital parameters (blue), and their combined effect (black). Units are W m^{-2}.

largest values are found in the model subtropics, where high surface temperatures and relatively low atmospheric humidity make the longwave emission more sensitive to greenhouse gas concentration.

Despite their importance in driving glaciation cycles, orbital parameter variations do not provide much radiative forcing at 21 kyr BP. There is a modest redistribution of solar radiation on an annual mean basis (due to the smaller obliquity relative to the present), with positive forcing in low latitudes and negative forcing at high latitudes. When decomposed seasonally, orbital parameter forcing is somewhat larger for certain latitudes and seasons, but remains modest because of the relatively small differences between the 21 kyr BP and modern orbital parameters.

The combined effect of these sources of radiative forcing is a pattern that has the largest forcing in the vicinity of the Northern Hemisphere ice sheets, where its magnitude exceeds 80 W m^{-2}, and the smallest forcing in the Tropics (Fig. 2), although small areas of large negative forcing occur in coastal regions where land has emerged due to the glacial reduction in sea level. Because of the powerful contribution of the surface albedo changes associated with the expansion of continental ice, the spatial pattern of combined forcing is very similar to that of the ice sheet forcing (not shown), with the CO_2 changes adding a quasi-uniform background forcing of -1.5 to -2.5 W m^{-2}. Thus the interhemispheric asymmetry of the surface albedo forcing is also characteristic of the combined forcing, with the spatially averaged forcing in the Northern Hemisphere (-5.92 W m^{-2}) being more than twice as large as in the Southern Hemisphere (-2.49 W m^{-2}).

Because the radiative effects of ice sheet expansion are confined to the extratropics, only three of these ra-

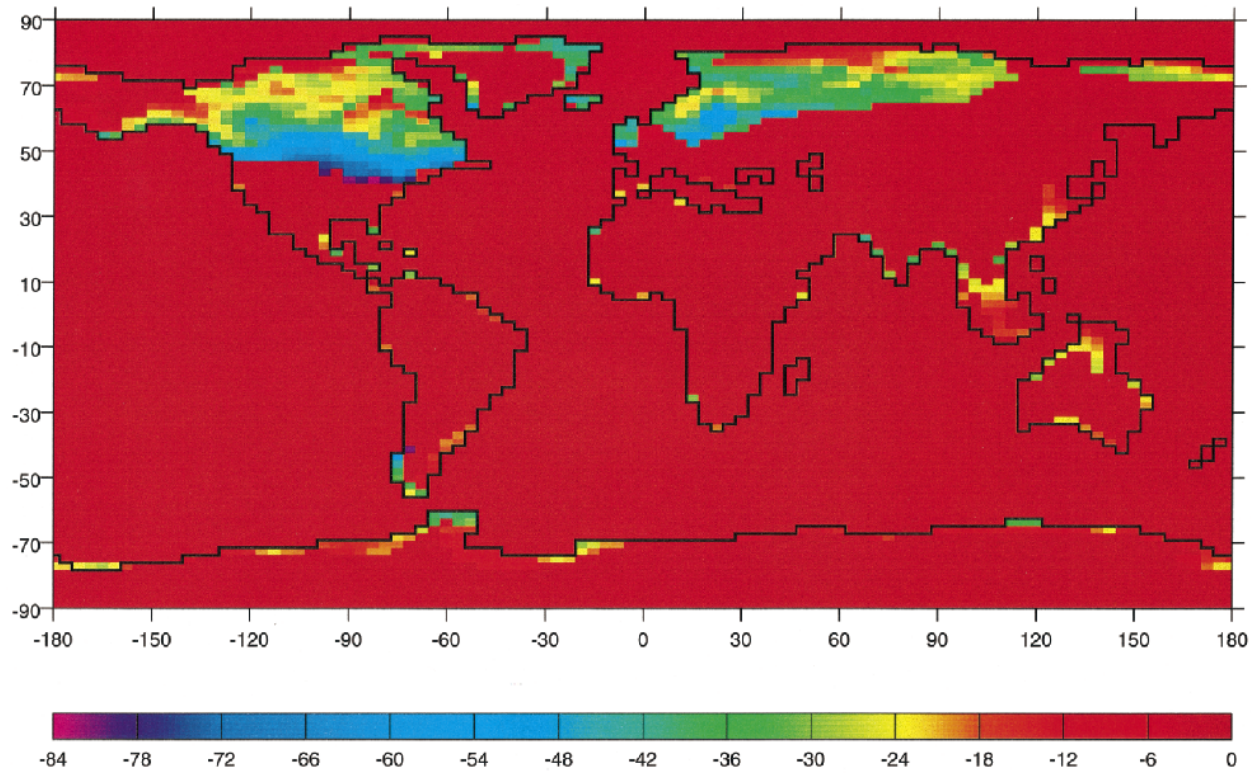

FIG. 2. Map of annual mean radiative forcing of LGM integration from the combined effects of sea level reduction, atmospheric CO_2, continental ice sheets, and orbital parameters. Units are W m^{-2} with color scale below.

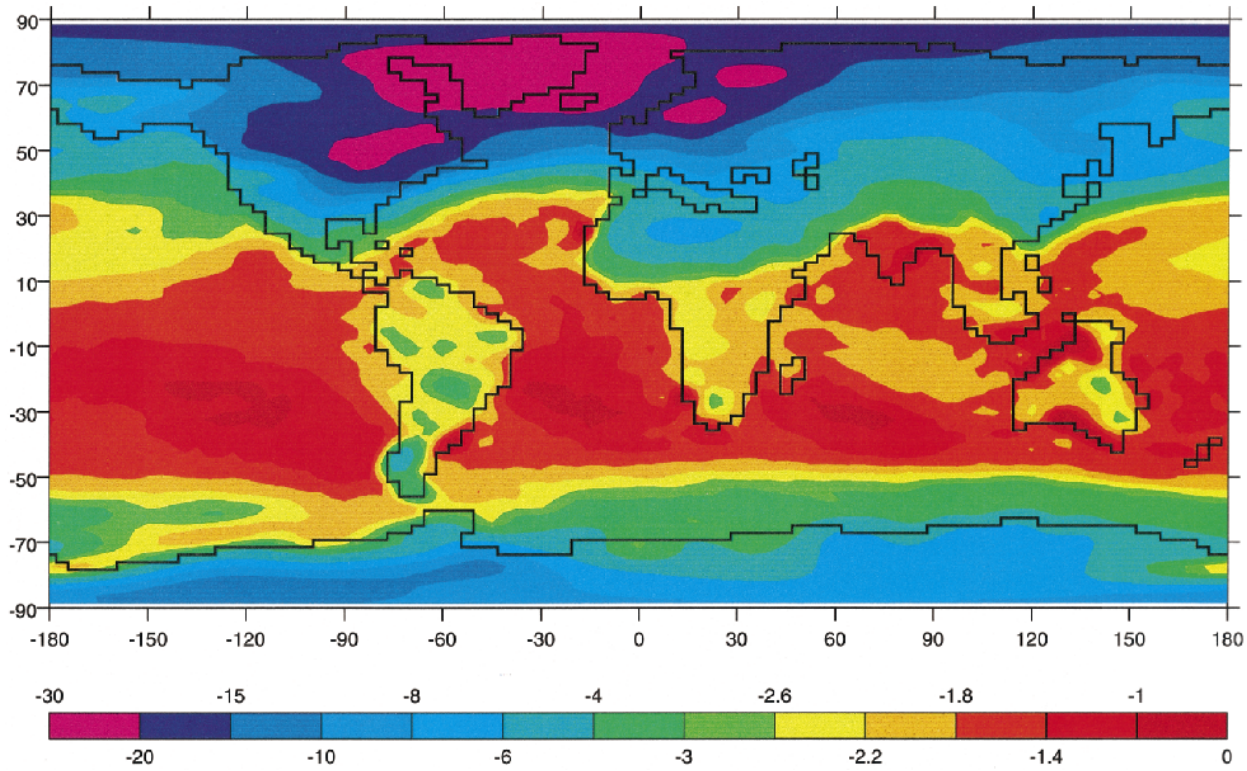

FIG. 3. Map of annual mean surface air temperature difference (ΔSAT) between LGM and modern integrations. Units are K with color scale below.

diative forcing mechanisms contribute to the overall forcing averaged over the tropical region (30°N–30°S). In this region, the radiative effects of orbital changes and sea level reduction nearly offset, leaving reduced CO_2 as the dominant forcing. The spatial nonuniformity of the sea level forcing results in a slight asymmetry about the equator, with the forcing of the northern Tropics being approximately 15% larger in magnitude than that of the southern Tropics.

Hewitt and Mitchell (1997) discuss the radiative forcing of an atmosphere–mixed layer ocean model simulation of the LGM climate conducted at the Hadley Centre. Their simulation also employs ice age boundary conditions specified by PMIP, making their results very suitable for comparison with the radiative forcing computed in this study. The primary factor complicating such a comparison is whether snow cover over the expanded ice sheets and emerged land points should be treated as a forcing or a feedback. For the purposes of this study, changes in snow cover are considered to be a feedback, so the radiative forcings from the LGM integration are compared with those from experiment ALB 1 of Hewitt and Mitchell (1997), in which snow cover was also treated as a feedback.

The combined global average radiative forcing of -4.4 W m^{-2} determined by Hewitt and Mitchell (1997) using experiment ALB1 is very similar to the -4.2 W m^{-2} forcing from the current study. In both sets of calculations, the ice sheet and CO_2 forcings are comparable in magnitude, although the contributions from these two components differ somewhat in detail. Compared to the results from this study, the ice sheet forcing of -2.3 W m^{-2} from the Hewitt and Mitchell (1997) model is ~0.4 W m^{-2} larger in magnitude, while their estimated CO_2 forcing of -1.7 W m^{-2} is ~0.3 W m^{-2} smaller. A number of factors may be involved in these differences, including the use of somewhat different methods to compute the forcing as well as differences in surface albedo parameterizations. The substantially smaller forcings due to sea level changes and orbital parameters are quite similar in both models.

5. Spatial patterns of simulated tropical cooling

A global view of differences in annual mean surface air temperature between the LGM and modern integrations (Fig. 3) shows some very broad similarity to the radiative forcing, as the simulated cooling is largest over and near the ice sheets. There are substantial differences between the patterns of forcing and temperature change, however, providing ample evidence that atmospheric dynamics and climate feedbacks have a significant effect on the response of the model.

Focusing on the Tropics, the reduction in surface air temperature averaged over the region from 30°N to 30°S is ~2 K (Table 2). Investigating the unforced variability

TABLE 2. Annually averaged surface air temperature difference (K) between LGM and modern integrations.

	Global	Northern Hemisphere	Southern Hemisphere	Tropics (30°N–30°S)	Northern Hemisphere Tropics (0°–30°N)	Southern Hemisphere Tropics (0°–30°S)
Land and ocean	−4.0	−5.9	−2.1	−2.0	−2.4	−1.7
Land only	−6.4	−7.9	−3.4	−2.7	−3.2	−2.2
Ocean only	−2.7	−4.1	−1.8	−1.7	−2.0	−1.5

of a similar A–MLO model, Manabe and Stouffer (1996) found the standard deviation of 25-yr mean surface air temperature anomalies to be less than 0.2 K throughout the Tropics. Thus the simulated LGM cooling represents a large signal relative to the background variability. The tropical cooling is not uniform; rather, it varies in magnitude from less than 1 K to more than 6 K. This spatial variability is illustrated by histograms depicting the frequency of annual mean surface air temperature difference (ΔSAT) at individual grid points between 30°N and 30°S (Fig. 4). The spatial variability in ΔSAT is greater over the continents, as evidenced by the long tail of the negatively skewed distribution for land points. The frequency distribution of ΔSAT over the oceans is more symmetric, but contains substantial variability nonetheless.

The spatial variability in ΔSAT is present on a variety of scales, from grid scale to hemispheric, and contributes to a rather complicated spatial distribution of ΔSAT. Nevertheless, there are some general patterns discernible amid this complexity that provide information about some of the mechanisms of climate change simulated by the model.

a. Interhemispheric asymmetry

On the largest scale, there is an asymmetry in the cooling of the two hemispheres, with the Northern Hemisphere average ΔSAT of −5.9 K greatly exceeding in magnitude the Southern Hemisphere average of −2.1 K. Similarly, the northern Tropics tend to cool more than the southern Tropics, as evident in the zonal averages of ΔSAT depicted in Fig. 5. Comparison of the hemispheric averages of ΔSAT (Table 2) and radiative forcing (Table 1) reveals that the ratio of these two quantities is nearly the same in each hemisphere, supporting the premise that the thermal response to radiative forcing is primarily realized in the hemisphere in which the forcing occurs. The tendency for in situ response within a hemisphere was originally noted by Manabe and Broccoli (1985a) in a climate simulation in which the only radiative forcing was provided by the LGM ice sheets and, thus, primarily restricted to the northern extratropics. They found that the thermal response in that simulation was almost exclusively confined to the Northern Hemisphere, as the negative radiative forcing due to the ice sheets was largely compensated by cooling within the hemisphere rather than an alteration of the interhemispheric heat transport. A similar conclusion was reached by Chen and Ramaswamy (1996) and Ramaswamy and Chen (1997) based on their analysis of integrations with spatially localized perturbations in cloud microphysical processes.

Thus it is likely that the greater overall cooling of the northern Tropics relative to the southern Tropics is

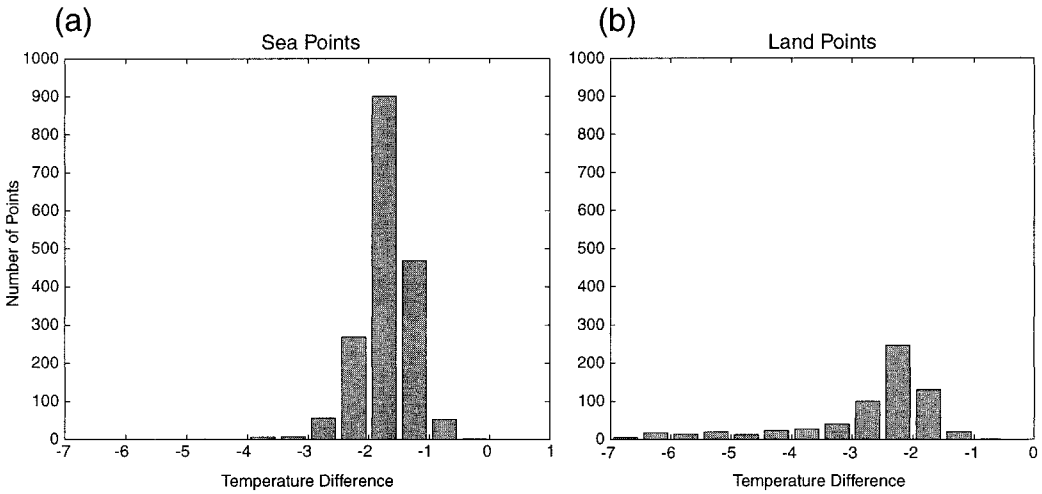

FIG. 4. Histograms depicting the spatial frequency distribution of the surface air temperature difference (ΔSAT) between LGM and modern integrations; ΔSAT is the abscissa and frequency (i.e., number of grid points) is the ordinate. Only grid points between 30°N and 30°S are considered: (a) ocean points, (b) land points.

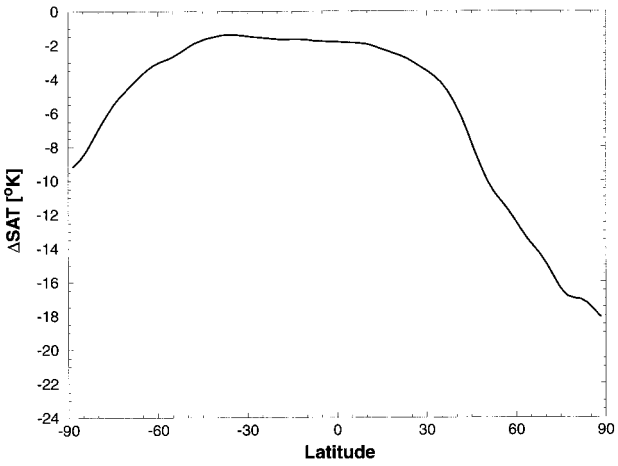

FIG. 5. Zonally averaged annual mean surface air temperature difference (ΔSAT) between LGM and modern integrations. Units are K.

a consequence of the contrast in radiative forcing between the hemispheres. Although the enhanced negative radiative forcing provided by the Northern Hemisphere ice sheets occurs exclusively in the northern extratropics, the effectiveness of atmospheric dynamical processes in mixing heat within a hemisphere results in a widespread cooling of the northern Tropics, leading to an interhemispheric asymmetry in tropical cooling. This asymmetry in thermal response has implications for atmospheric circulation, as will be discussed in a subsequent section.

b. Land–ocean contrast

Another source of variation in ΔSAT on relatively large scales is the tendency for greater cooling over the continents. In the region from 30°N to 30°S, the cooling over land points averages 2.7 K as compared to 1.7 K over ocean points (Table 2). Although this difference in ΔSAT is modest, it represents a substantial fraction of the area-averaged tropical cooling. Two mechanisms are most important in explaining this tendency for greater cooling over land.

First, the lowering of sea level at the LGM results in an increase of land elevation (relative to ocean elevation) of ~84 m averaged from 30°N to 30°S. (This differs from the prescribed sea level change of 105 m due to the smoothing associated with the spectral representation of topography.) Given the general decrease of temperature with elevation, this mechanism might be expected to account for approximately half of the difference in cooling (0.084 km × 6 K (km)$^{-1}$ = ~0.5 K) if the decrease in temperature with height were assumed to occur at the moist-adiabatic lapse rate. Results from the LGM-NE integration, identical to the LGM integration except without the prescribed lowering of sea level, indicate that the land–sea difference in cooling is reduced from 1.0 K to 0.5 K (Table 3), confirming the importance of the elevation effect.

TABLE 3. Annual mean surface air temperature difference (K) between LGM integration and LGM-NE integration for the region from 30°N to 30°S.

	Land and ocean	Land only	Ocean only
ΔSurface Air Temperature	−0.05	−0.41	+0.10

The second mechanism responsible for the greater cooling over land involves the surface energy balance. Any radiatively induced perturbation in the energy balance must be compensated by some combination of sensible and latent heating of the atmosphere. Differences in moisture availability between land and ocean affect the manner in which these two surface types respond to radiative forcing. Over ocean surfaces, the unlimited availability of moisture allows latent heating to compensate for most of a given perturbation in the energy balance. Since the latent heat does not produce in situ heating of the atmosphere, the compensation can be accomplished with a relatively small change in surface air temperature. Over land, changes in sensible heating must compensate for a greater fraction of the radiatively induced perturbation in the energy balance, resulting in greater sensitivity of surface air temperature.

c. Advective effects

An additional source of spatial variability in ΔSAT is associated with the substantial changes in atmospheric circulation that occur in the LGM simulation. Although the largest changes in surface circulation occur in the middle and high latitudes of the Northern Hemisphere, surface winds are also altered at low latitudes, particularly in the northern Tropics and subtropics (Fig. 6a). Changes in horizontal thermal advection accompany the changes in surface winds, offering the potential for regional variations in the amount of LGM cooling.

To evaluate the importance of this mechanism, changes in near-surface thermal advection are estimated by computing the quantity $-\Delta\mathbf{V} \cdot \nabla T$, where $\Delta\mathbf{V}$ is the difference in the annual mean vector wind between the LGM and modern integrations and T is determined by averaging the annual mean surface air temperature of the LGM and modern integrations. This quantity is depicted in Fig. 6b. Positive (negative) values of $-\Delta\mathbf{V} \cdot \nabla T$ indicate that changes in surface circulation contribute to an advective warming (cooling).

Relationships between ΔSAT and $-\Delta\mathbf{V} \cdot \nabla T$ are evident, particularly over the oceans. Anomalous northeasterly winds over the central North Pacific between the equator and 20°N result in an advective cooling effect that enhances the temperature reduction in that region. Similarly, the advective cooling associated with southerly component flow over the south-central Indian Ocean and just west of Australia contributes to enhanced cooling there. Over land, the enhanced northerly flow

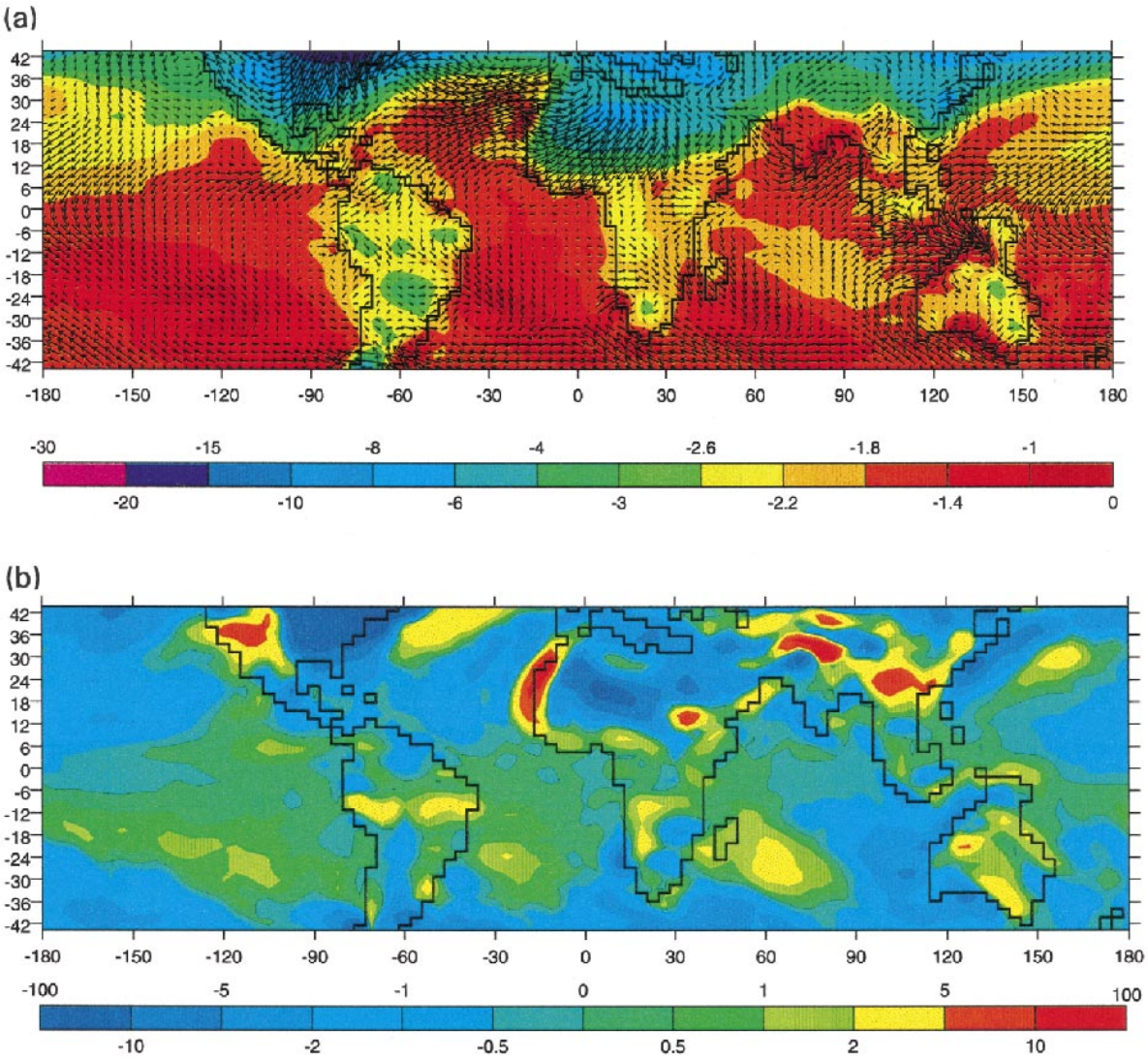

FIG. 6. (a) Map of annual mean surface air temperature difference (ΔSAT) between LGM and modern integrations (units are °C, color scale below) with vector difference in surface winds superimposed. (b) The quantity $-\Delta\mathbf{V}\cdot\nabla T$, where $\Delta\mathbf{V}$ is the difference in the annual mean vector wind between the LGM and modern integrations and T is determined by averaging the annual mean surface air temperature of the LGM and modern integrations. Units are 10^{-6} K s^{-1} with color scale below. Positive (negative) values of $-\Delta\mathbf{V}\cdot\nabla T$ indicate that changes in surface circulation contribute to an advective warming (cooling).

over northern Africa and southern North America results in negative values of $-\Delta\mathbf{V}\cdot\nabla T$ and contributes to the relatively large cooling that prevails in these areas.

Advective effects are also associated with the regions of low temperature sensitivity oriented from west-northwest to east-southeast over portions of the subtropical South Atlantic, South Indian, and South Pacific Oceans. Anomalous poleward (i.e., northerly component) flow results in advective warming over these regions, thus reducing the magnitude of ΔSAT. As a consequence, the simulated LGM cooling is substantially smaller than the tropical mean, being generally less than 1 K. Advective warming also contributes to the swath of reduced cooling that extends from the Philippine Islands northeastward toward the area around 30°N and the date line.

Evidence from other climate modeling experiments suggests that the interhemispheric asymmetry in the LGM cooling may be responsible for some of the surface wind anomalies that lead to the advective effects described in this section. Specifically, a reorientation of the Hadley circulation occurs in which the rising branch is displaced toward the hemisphere that experiences a warming relative to its counterpart. In the LGM integration, the smaller cooling of the Southern Hemisphere relative to the Northern Hemisphere (see Table 2) leads to a southward displacement of the rising branch of the Hadley cell and a tendency for anomalous northerly flow across the equator. Other changes in surface circulation also accompany this change in the meridional circulation.

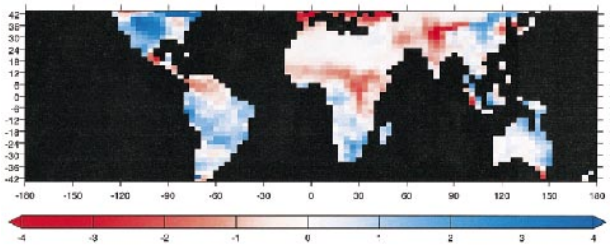

FIG. 7. Map of annual mean soil moisture difference between LGM and modern integrations. Units are cm with color scale below.

d. Other sources of small-scale variation

Changes in soil moisture also influence the spatial distribution of ΔSAT over the continents through their effect on the surface energy budget. For example, areas that experience an increase in soil moisture cool relative to those in which there is no change in soil moisture, as the wetter soil alters the partitioning of energy available at the surface between sensible and latent heating such that the Bowen ratio is reduced. The reduction in sensible heating of the lower troposphere leads to a decrease of surface air temperature. This mechanism appears to be responsible for areas of enhanced cooling over interior South America near 20°S, southern Africa, and northeastern Australia, where soil is wetter in the LGM simulation (Fig. 7).

Conversely, decreases of soil moisture are accompanied by a relative warming, as the decreased availability of water causes the surface energy budget to shift toward greater sensible heating of the atmosphere. The regions of relatively small cooling over central equatorial Africa and extreme northwestern South America are associated with decreased LGM soil moisture.

Through the same mechanism, the replacement of ocean in the modern integration with land in the LGM integration causes some areas to have substantially reduced LGM cooling. This occurs along the continental margins where the glacial sea level lowering exposed continental shelf regions currently under water. For there to be a substantial thermal effect, these locations must be relatively dry so their moisture availability is significantly lower than that of an ocean grid point. Such dryness occurs over the west coast of southern Africa, the west shore of the Bay of Bengal, and northwestern Australia–New Guinea. The latter region experiences the smallest change in surface air temperature anywhere in the Tropics. For the most part, this phenomenon is relatively local and has little influence on the area-averaged temperature change. While of some importance in understanding the distribution of temperature change simulated by the model, these regions of reduced cooling would be difficult to identify from paleoclimatic data. The enormous environmental change associated with the transition from land to ocean would probably prevent whatever air temperature changes may have occurred from being evident in the geological record.

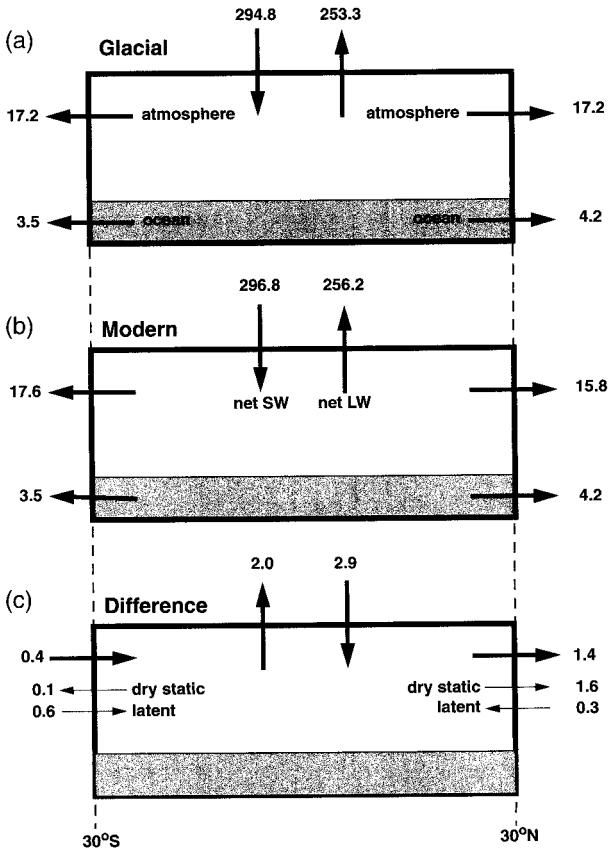

FIG. 8. Schematic diagram of annual mean energy budget for the latitude belt from 30°N to 30°S. Labeled arrows indicate the direction and magnitude of the energy fluxes. Energy transports through the northern and southern boundaries are expressed as the equivalent energy fluxes over this latitude belt. Units are W m^{-2}. (a) LGM simulation. (b) Modern simulation. (c) Difference (LGM-modern).

6. Tropical energy balance

Changes in the energy balance of the Tropics caused by the radiative forcing associated with LGM boundary conditions and the response of the climate to that forcing can provide insights into the maintenance of LGM tropical temperatures. Figure 8 contains schematic diagrams illustrating the energy balance of the latitude belt extending from 30°S to 30°N. At the top of the atmosphere, net shortwave radiation for both the modern and LGM simulations exceeds the net longwave emission. This energy surplus is balanced by an export of energy into the extratropics, shared between the atmosphere and the ocean, across the boundaries at 30°S and 30°N. The oceanic component of this flux to the extratropics is uniquely determined by the heat flux adjustment, which is prescribed to mimic the horizontal heat transport by the ocean. Comparing the simulated energy export in the modern simulation to observational estimates, the total heat flux is very similar to observations. In some observational estimates, the magnitude of the atmospheric component is smaller than that of the model,

but the wide variation among estimates makes it difficult to assess the importance of the disagreement.

When examining the changes in the energy balance between the LGM and modern simulations, one should recognize that the meridional heat transport associated with the heat flux adjustments has been constrained to be identical in the modern and LGM integrations at every latitude, as discussed in section 3. Thus any alteration in the balance between the net shortwave and longwave radiation at the top of the tropical atmosphere must be compensated by an alteration in the meridional heat transport by the atmosphere, since only that component of the heat flux to the extratropics is free to change in response to the imposition of LGM forcing.

Changes in the radiation balance at the top of the atmosphere occur in response to glacial forcing, as evident in the differences in energy balance components between the LGM and modern integrations (Fig. 8, bottom). The cooling of the tropical atmosphere with respect to the modern integration and associated feedbacks lead to a decrease in longwave emission at the top of the atmosphere of 2.9 W m^{-2}. Cloud cover changes are only responsible for a relatively small fraction of this decrease. An offline computation of clear-sky radiative fluxes indicates an emission decrease of 2.0 W m^{-2}, suggesting that changes in temperature, water vapor, and atmospheric CO_2 are responsible for most of the decrease of outgoing longwave radiation from the Tropics in the LGM integration.

For the tropical energy balance to be maintained, this gain of 2.9 W m^{-2} relative to the modern integration must be offset by a loss of equal magnitude. Part of the needed loss is provided by a decrease in net shortwave radiation of 2.0 W m^{-2}. There are a number of factors that contribute to the change in this quantity. The additional land area in the LGM integration resulting from the lowering of sea level contributes a radiative forcing of -0.6 W m^{-2} by raising the area-averaged surface albedo, but this is almost entirely offset by a radiative forcing of $+0.5$ W m^{-2} that results from the small differences in orbital parameters (Fig. 1). Without a substantial contribution from these radiative forcings, the decrease in net shortwave radiation must result from responses internal to the climate system. Clouds and snow cover offer the most potential to alter the shortwave budget. Of the two, cloud changes are more important in the Tropics, as clear-sky shortwave flux calculations indicate a decrease of only 0.6 W m^{-2}, indicating that cloud changes account for 1.4 W m^{-2}, or more than two-thirds of the decrease in top-of-atmosphere radiation. The remainder of the decrease in net shortwave radiation stems from an increase in snow cover over the interior of North America and Eurasia, which extends equatorward of 30°N during the winter season, particularly near and just east of the Tibetan Plateau.

The remaining energy loss is satisfied by an increase in the net atmospheric energy transport to the extratropics. An increase of 1.4 W m^{-2} across 30°N more than offsets a decrease of 0.4 W m^{-2} across 30°S, so that the net atmospheric export increases by 1.0 W m^{-2}. (Note that the energy transport is expressed as the energy flux per unit area for the tropical band between 30°N and 30°S. To obtain the energy transport in the more conventional units of power, the flux per unit area must be multiplied by area of this band, which is 2.55×10^{14} m^2.) When decomposed into the contributions from dry static energy and latent heat, the increase in atmospheric heat transport results from opposing mechanisms. Latent energy transport decreases in both hemispheres in response to the overall reduction in atmospheric water vapor content. In contrast, the transport of dry static energy increases, most notably in the Northern Hemisphere. This is likely to be a consequence of the steepened pole-to-equator temperature gradient there. Only a very small increase of dry static energy transport occurs in the Southern Hemisphere, where there is little change in the pole-to-equator temperature gradient in the vicinity of 30°S.

7. Comparison with paleodata

In this section, the glacial temperature changes simulated by the A–MLO model are compared with paleotemperature reconstructions to determine the degree of similarity between estimates of temperature change from these two sources. The comparison will focus on the region between 35°N and 35°S to include the subtropics as well as the deep Tropics. The method of Broccoli and Marciniak (1996) is used, in which comparisons are made at only the specific geographical locations where the paleodata are available. In order for the comparisons to take place at comparable spatial scales, both the paleodata and model output are represented as anomalies on a common grid, which is chosen to be the model's 2.25° lat × 3.75° long grid. For each of these grid boxes, a glacial temperature anomaly is defined only if there is a paleotemperature estimate located within its boundaries. If more than one estimate falls within the box, the individual values from these estimates are averaged to form the anomaly. The result is a gridded analysis in which glacial paleotemperature anomalies are defined only at a subset of the model grid points. Output from the model is also sampled at only those locations for which paleotemperature reconstructions exist. Sampling the paleodata in this way avoids the errors associated with extending analyses to areas of sparse data coverage and makes the uncertainties associated with inadequate spatial sampling more evident.

a. CLIMAP SST reconstructions

The CLIMAP project (CLIMAP Project Members 1981) reconstructed SSTs for the LGM by determining the present-day relationships between the abundances of various species of marine microorganisms and the

temperatures of the near-surface ocean waters they inhabit, then applying those relationships to past periods by examining the shells deposited in deep sea sediment cores. The relationships are expressed quantitatively through the use of multiple regression transfer functions in which the predictand is SST and the predictors are empirical orthogonal functions of species abundances. Although questions have been raised about the CLIMAP reconstruction (Webster and Streten 1978; Rind and Peteet 1985; Guilderson et al. 1994) and specific revisions have been suggested during the time since its compilation (e.g., Anderson et al. 1989), this study uses the original CLIMAP dataset, which remains the only near-global SST database for the LGM.

To prepare the input for the procedure described at the beginning of this section, estimates of anomalies are needed at the specific locations where the paleodata were collected. To obtain these locations, the digitized global subjective analyses were sampled at the core locations listed in the CLIMAP atlas (CLIMAP Project Members 1981). The February and August values at each location, intended to represent the thermal extremes of the two hemispheres, were then averaged to estimate an ''annual mean'' SST anomaly. For consistency, the simulated LGM-modern SST differences for February and August were also averaged in the same way.

The glacial SST anomalies reconstructed by CLIMAP vary widely over the region from 35°N to 35°S, with values from −7.9 K to +2.8 K (Fig. 9a). The cooling is largest in the North Atlantic, where the anomalies at most locations range from −2 to −5 K. Negative anomalies with magnitudes in excess of 6 K are adjacent to the North African coast, indicative of enhanced LGM upwelling there (CLIMAP Project Members 1981). Anomalies of −1 to −3 K are typical in the Gulf of Mexico and the Caribbean Sea. In the South Atlantic the glacial cooling is not quite as large, ranging from −2 to −4 K in the east to near zero in the western subtropical South Atlantic. A number of regional patterns are evident in the Pacific. An anomaly gradient extends across the equatorial Pacific, with anomalies of −2 to −3 K in the western warm pool, small negative anomalies in the central Pacific, and small positive anomalies in the east (except −1 to −3 K in the near-coastal waters). Positive SST anomalies are found in the subtropical gyres of the North and South Pacific, although the data are sparsely distributed, particularly in the North Pacific. The western Indian Ocean also exhibits anomalies that are either positive or near zero, while small negative anomalies predominate in the eastern Indian Ocean. Larger negative anomalies (−2 to −4 K) are found in the subtropical south Indian Ocean. These have been interpreted as indicative of an equatorward shift in oceanic fronts in this region.

Simulated changes in annual mean SST between the LGM and modern simulations are depicted in Fig. 9b. The spatial variability of the simulated SST anomalies is smaller than that found in the CLIMAP reconstructions. Unlike the CLIMAP paleotemperatures, the simulated changes are negative throughout the entire region from 35°N to 35°S, with a cooling of between 1–2 K covering most of this region. The cooling is somewhat smaller in the Southern Hemisphere, with the smallest changes of approximately −1 K occurring in the subtropical South Pacific, South Atlantic, and south Indian Oceans. This is consistent with the ΔSAT pattern described in section 5. Perhaps coincidentally, the region of small cooling in the subtropical South Pacific occupies one of the regions in which CLIMAP found little organism response, as evidenced by the slight warming in reconstructed SST. Elsewhere, cooling of 2 K or more is widespread through much of the North Atlantic, with the largest cooling in coastal regions adjacent to North America and northern Africa, where offshore flow prevails.

To facilitate the identification of spatial variations in the agreement or disagreement between the LGM simulation and the CLIMAP reconstruction, the algebraic difference between the simulated glacial SST anomaly and the CLIMAP reconstruction at each grid point is considered (Fig. 9c). This ''model–paleodata discrepancy'' is relatively small (±1 K) over much of the Atlantic, western tropical Pacific, and the Bay of Bengal region. Large positive discrepancies appear in coastal regions adjacent to northern Africa, Namibia, and western Australia, and also in the south Indian Ocean south of Madagascar. Because the A–MLO model lacks ocean dynamics, the large discrepancies in the aforementioned coastal regions may be due to the inability of the ocean model to respond to strengthened trade winds by producing enhanced upwelling. Large negative discrepancies appear over the subtropical and eastern tropical Pacific, as well as the Arabian Sea and western tropical Indian Ocean. In many of these regions, the large negative values arise as the result of a disparity in the sign of the glacial SST anomaly, with the simulated cooling contrasting with the positive anomalies reconstructed by CLIMAP. The significance of the disagreement in these regions is somewhat unclear, however, as the discrepancies are comparable in magnitude to the standard errors of the transfer functions used to derive the CLIMAP reconstructions. Prell (1985) has determined these errors to be as large as 3 K in the Pacific and Indian Oceans. Recently, Lee and Slowey (1999) inferred a 2-K cooling of the subtropical North Pacific from oxygen isotopes and species compositions of surface-dwelling organisms in a core near Hawaii. The result is in sharp contrast with the nearly 2-K warming reconstructed by CLIMAP for a nearby site.

The annual mean CLIMAP SST anomaly averaged over the region from 35°N to 35°S is −1.4 K. When sampled at the same grid points and spatially averaged, the simulated SST anomaly is −1.8 K, indicating that the model is only slightly colder overall than the CLIMAP reconstruction in low latitudes. This overall sim-

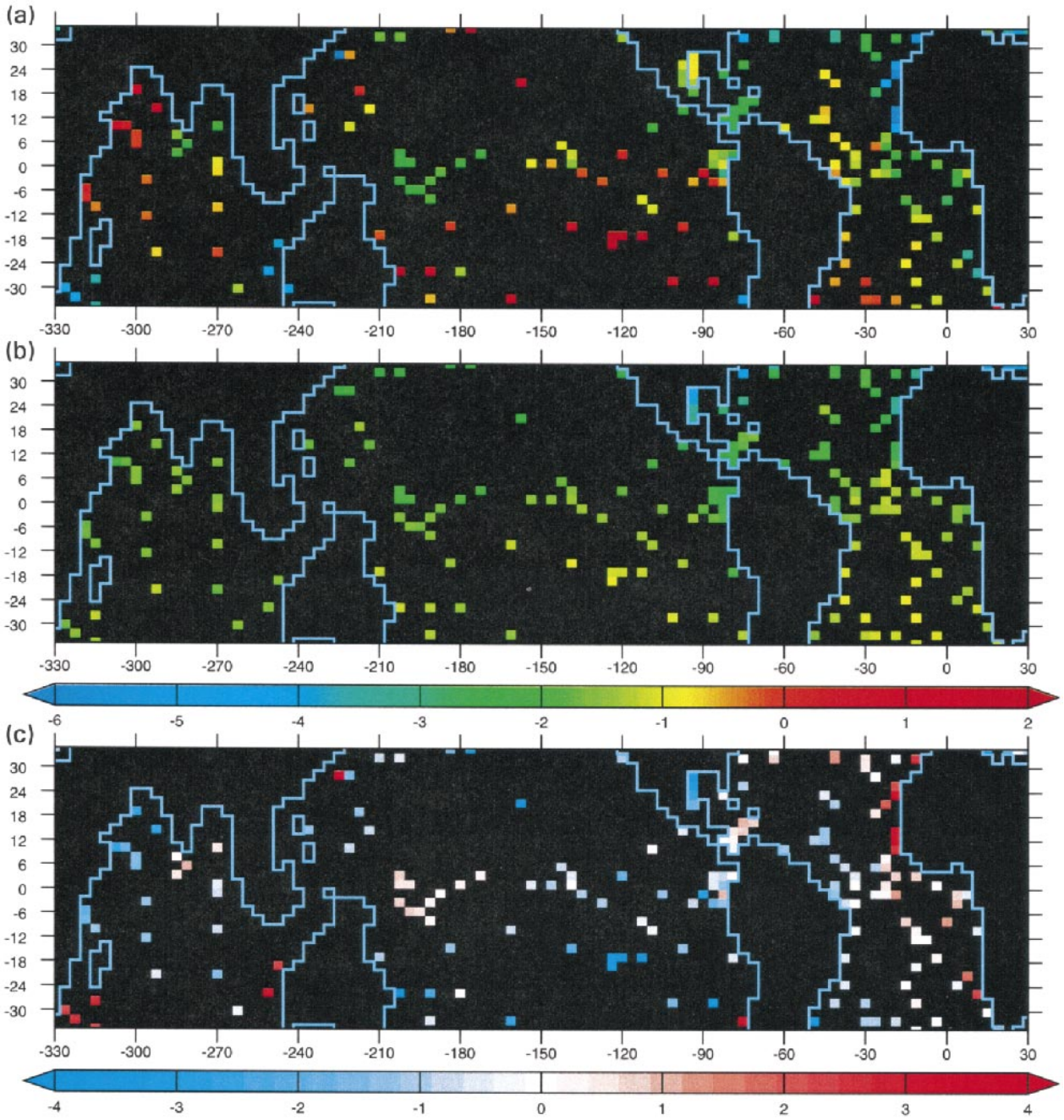

FIG. 9. (a) Difference in annual mean sea surface temperature (SST) between LGM and present as reconstructed by CLIMAP. (b) Difference in annual mean SST between LGM and modern integrations. (c) Model–paleodata discrepancy (i.e., the algebraic difference between the simulated and reconstructed SST differences). Units are K. Color scale for top and center panel is below center panel; color scale for bottom panel is below bottom panel. Grid boxes are colored only if they contain at least one paleotemperature estimate.

ilarity between the model and CLIMAP SSTs is also evident in the zonal averages (Fig. 10a). Interbasin differences are also apparent when zonal averages are computed separately for each ocean (Figs. 10b–d), with the best agreement in the Atlantic and the poorest agreement in the Pacific. These results are very similar to those obtained by Broccoli and Marciniak (1996) from an ice age simulation experiment that differed from the current experiment both in model formulation and LGM forcing, as discussed in sections 2 and 3. As discussed by Broccoli and Marciniak (1996), the interbasin differences are such that the best agreement occurs in that

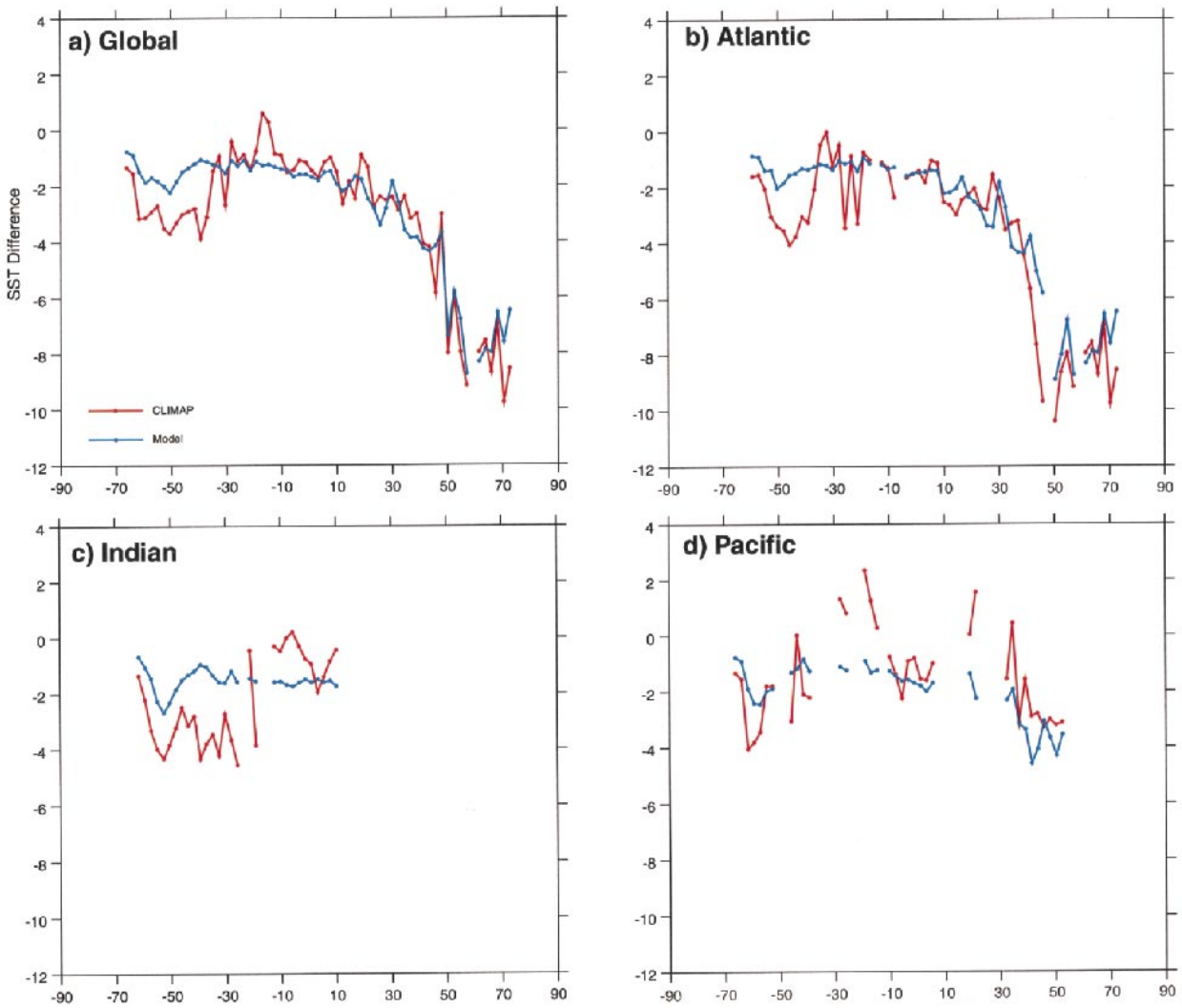

FIG. 10. Zonally averaged annual mean difference in sea surface temperature between LGM and present as reconstructed by CLIMAP (red) and simulated by model (blue). Units are K. (a) Global, (b) Atlantic, (c) Indian, and (d) Pacific.

basin in which estimation errors are small and the sampling density is high, while the poorest agreement occurs where the estimation errors are large and the sampling density is low. The tendency for the largest discrepancies to occur where the uncertainties are also large makes it difficult to assert that the regional differences between the model and CLIMAP glacial SST anomalies have physical significance.

b. Modern analog SST reconstructions

Prell (1985) utilized a different method to determine glacial SSTs from the species abundances of marine microfossils in deep sea sediment cores. This method, known as the modern analog technique, uses statistical measures of dissimilarity to find the samples in a database of sediment core tops (i.e., the modern analogs) whose species composition most resembles that of a particular LGM sample. Once these modern analogs are identified, the modern SST values at the same locations are averaged to produce an estimate of glacial SST. Prell (1985) describes a number of advantages and disadvantages associated with the modern analog technique, but of most importance to this study is that it represents a way to extract paleoceanographic information from species compositions that is distinctly different from the transfer function method used by CLIMAP. One should note, however, that the modern analog technique and the transfer function method both utilize information about the species composition of marine microorganisms to infer SSTs.

The modern analog technique reconstructions are expressed as SST anomalies for the warm season and cold season at each of the locations at which LGM samples were available in a set of sediment cores taken primarily from the CLIMAP database and supplemented by ad-

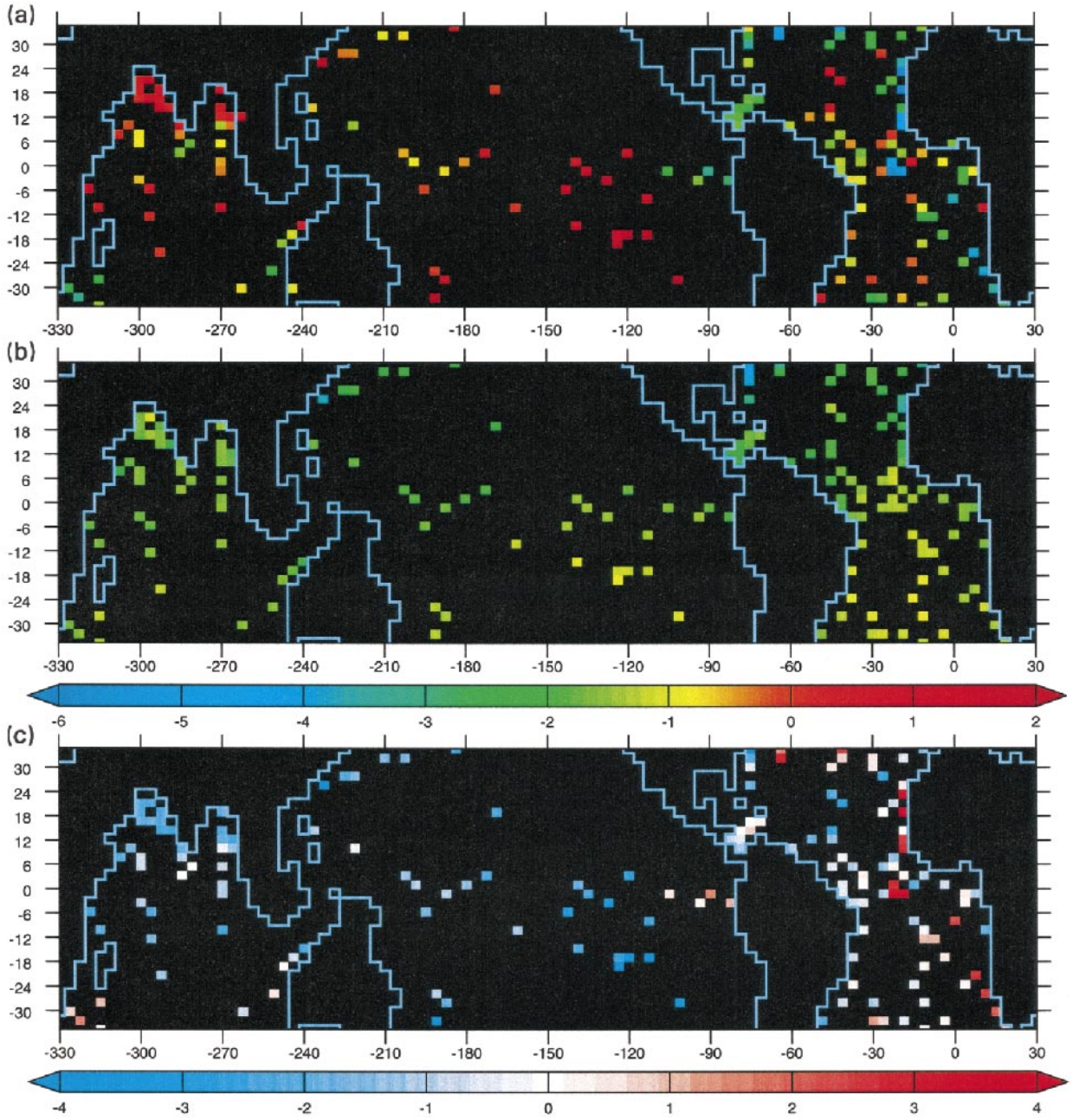

FIG. 11. Same as Fig. 9 except paleotemperature data are modern analog SST reconstructions from Prell (1985).

ditional samples from the Indian Ocean. The core locations and reconstructed glacial SST anomalies are taken from Prell (1985, Table 9). As in the case of the CLIMAP estimates, the warm and cold season anomalies at each location are averaged to estimate an annual mean SST anomaly.

The glacial SST anomalies reconstructed using the modern analog technique are depicted in Fig. 11a. Differences in the spatial distribution of SST estimates are evident in comparison to the CLIMAP estimates, most notably the increased data density in the North Indian Ocean and the decreased data density in portions of the Pacific. These differences in spatial sampling are consistent with the emphasis on the regions of positive glacial SST anomalies in the CLIMAP reconstruction, a primary goal of the Prell (1985) study. As in the CLIMAP estimates, the glacial Atlantic is relatively cool except for small positive anomalies midway between the Lesser Antilles and Africa and at scattered sites elsewhere. Rather large negative anomalies (-4 K) are evident along the coast of North Africa, another similarity with the CLIMAP reconstruction. The Pacific is

dominated by anomalies that are either near zero or positive, with the positive anomalies particularly evident in the central equatorial Pacific and the southern subtropical gyre. Along the equatorial belt, the modern analog reconstructions are warmer than CLIMAP from the western warm pool eastward through 120°W. In the densely sampled north Indian Ocean, anomalies of ±1 K are found in both the Arabian Sea and the Bay of Bengal. Elsewhere, the area south of Madagascar contains substantial negative anomalies, a feature in common with the CLIMAP estimates.

Because the spatial distribution of modern analog paleotemperatures is quite similar to that of CLIMAP, the spatial patterns of simulated glacial SST anomalies when sampled at the locations of the modern analog estimates (Fig. 11b) are virtually identical to those described in the previous subsection. Computation of the model–paleodata discrepancy, or difference between the simulated and modern analog technique anomalies (Fig. 11c), indicates relatively good agreement in the Atlantic where most values are ±1°C. Exceptions appear in the subtropical coastal regions adjacent to Africa in both hemispheres, where the model is relatively warm, and midway between the Lesser Antilles and Africa, where a sizeable negative discrepancy is noted. Positive discrepancies in excess of 2 K also exist in the equatorial Atlantic midway between South America and Africa. The existence of positive discrepancies in regions of modern upwelling may be associated with the inability of the simple oceanic component of the model to simulate enhanced upwelling, as discussed in the previous subsection. Negative discrepancies predominate in the Indian and Pacific Oceans, with the largest magnitudes in the Bay of Bengal, the central equatorial Pacific, and the subtropical gyres of the North and South Pacific.

When averaged over the region from 35°N to 35°S, the annual mean SST anomaly reconstructed by the modern analog technique is −1.0 K. This is slightly warmer than the CLIMAP average, with the difference probably resulting from a combination of greater emphasis on the positive anomaly regions and methodological differences. When sampled at the same grid points, the spatially averaged SST anomaly simulated by the model is −1.7 K, indicating that the model is slightly colder than the modern analog estimates in low latitudes. Zonally averaged SST anomalies also reveal this small systematic difference (Fig. 12a). Important interbasin differences can also be discerned from the zonal averages (Figs 12b–d), with the negative discrepancies in the Indian and Pacific Oceans having considerably larger magnitude than in the Atlantic. As in the cases of the CLIMAP estimates, the better spatial coverage in the Atlantic allows that basin to dominate the zonal means computed from all basins combined.

c. Alkenone SST reconstructions

A more recently developed method for reconstructing SST uses alkenone molecules that are produced by plankton and preserved in marine sediments. A strong empirical relationship exists between the ratio of two different types (diunsaturated and triunsaturated) of alkenone molecule and the temperature at which the plankton grew (Brassell et al. 1986). By examining this ratio in deep-sea sediment cores, a history of SST can be extracted.

The number of alkenone estimates of glacial SST has increased rapidly during the last several years as this technique has become more widely available. The Sea Surface Temperature Evolution Mapping Project (TEMPUS) has compiled a set of alkenone SST estimates for the LGM from a number of sites using a variety of sources, primarily existing publications (Rosell-Melé et al. 1998). At the time of this writing, specific references for these sources, along with the site locations and paleotemperature estimates, are available at the TEMPUS Project Internet site (http://nrg.ncl.ac.uk:8080/climate/Tempus.htm). The alkenone paleotemperatures are expressed as anomalies of annual mean SST, which serve as input to the procedure described at the beginning of this chapter.

Figure 13a reveals that the distribution of alkenone SST estimates is quite inhomogeneous, with most sites located in coastal regions of the Atlantic and north Indian Oceans, and vast areas in the oceanic interiors almost completely devoid of data. Most of the glacial SST anomalies reconstructed by this method are in the range from −1 to −5 K. Anomalies in the eastern portions of the Atlantic are comparable to the other SST estimates, with most sites in the range from −2 to −5 K. The alkenone estimates from the north Indian Ocean are somewhat cooler than those resulting from the CLIMAP or modern analog reconstructions, primarily ranging from −1 to −3 K. The warmest anomalies are at two grid points in the central and eastern equatorial Pacific, where the glacial SST change is estimated to be negligible. Some cooling is estimated for a grid point north of New Guinea, suggesting an SST anomaly gradient across the equatorial Pacific that bears some resemblance to those estimated by CLIMAP and the modern analog technique of Prell (1985).

In most locations, the SST anomalies simulated by the A–MLO model (Fig. 13b) are quite similar in magnitude to the alkenone estimates when sampled at the same locations. The simulated cooling varies from 1 to 5 K, with most values toward the low end of this range. Locations in the North Atlantic cool by 2–5 K, while the more numerous sites in the equatorial and South Atlantic cool by between 1 and 2 K. In the Indian Ocean, the anomalies are generally between −2 and −3 K. Most of the computed discrepancies between the simulated and alkenone SST anomalies are relatively small, particularly in the Indian Ocean. A mixed pattern appears in the Atlantic, with a slight positive tendency and no regional patterns discernible. The model is generally colder than the alkenone estimates across the central and eastern equatorial Pacific. Overall, the spatially av-

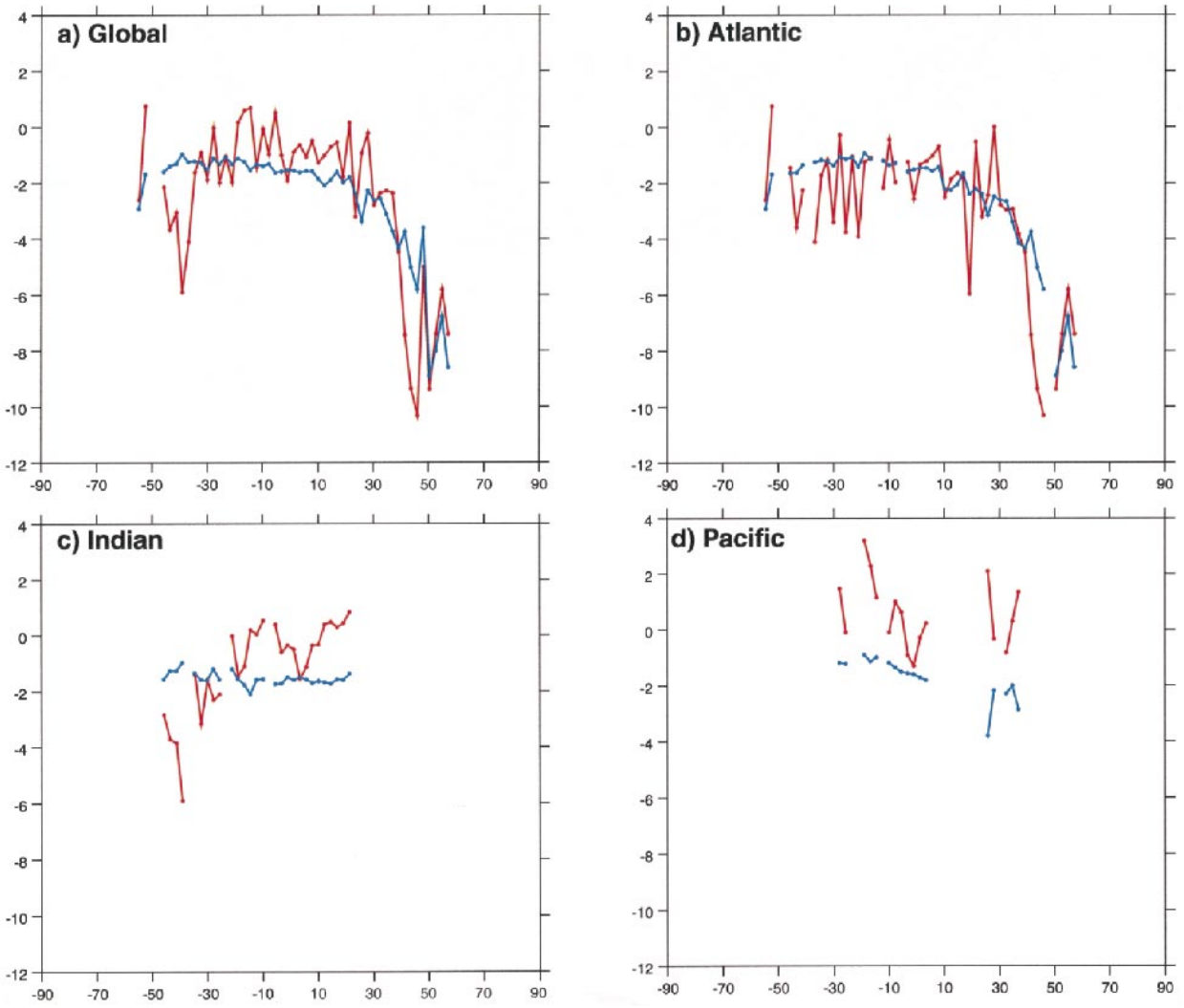

FIG. 12. Same as Fig. 10 except paleotemperature data are modern analog SST reconstructions from Prell (1985).

eraged annual mean SST anomaly estimated from alkenones for the low latitude (35°N–35°S) region is −2.3°C, which is slightly colder than the simulated value of −1.9 K.

d. Noble gases in groundwater

A geochemical method for reconstructing terrestrial temperatures involves the measurement of noble gases (i.e., neon, argon, krypton, and xenon) dissolved in groundwaters taken from deep aquifers (Stute and Schlosser 1993). Because the solubilities of these gases are temperature dependent, their concentrations record the temperature of the water table from which the aquifer is charged. Under the correct geological conditions, groundwater of glacial age may be available that has been isolated from more recent surface conditions. Since the noble gases are chemically inert, their relative concentrations can be assumed to be invariant from the time the groundwater was part of the near-surface water table. Because of the damping of the seasonal and diurnal temperature cycles with depth, the noble gas method yields an estimate of the mean annual ground temperature. Paleotemperature estimates based on the noble gas method are used as input to the procedure described at the beginning of this section (Heaton et al. 1986; Stute et al. 1992, 1995a,b; Clark et al. 1997). Simulated changes in annual mean land surface temperature from the A–MLO model constitute the comparison dataset.

Only five estimates of noble gas paleotemperatures are available in the region from 35°N to 35°S, so regional patterns cannot be readily discerned (Table 4). Furthermore, the noble gas temperature anomalies are rather uniform, ranging from −4 to −5.5 K. The simulated land surface temperature anomalies occupy a wider range between −2 and −7 K, with the largest cooling within this region occurring in southern North America, the smallest cooling in southern Africa, and

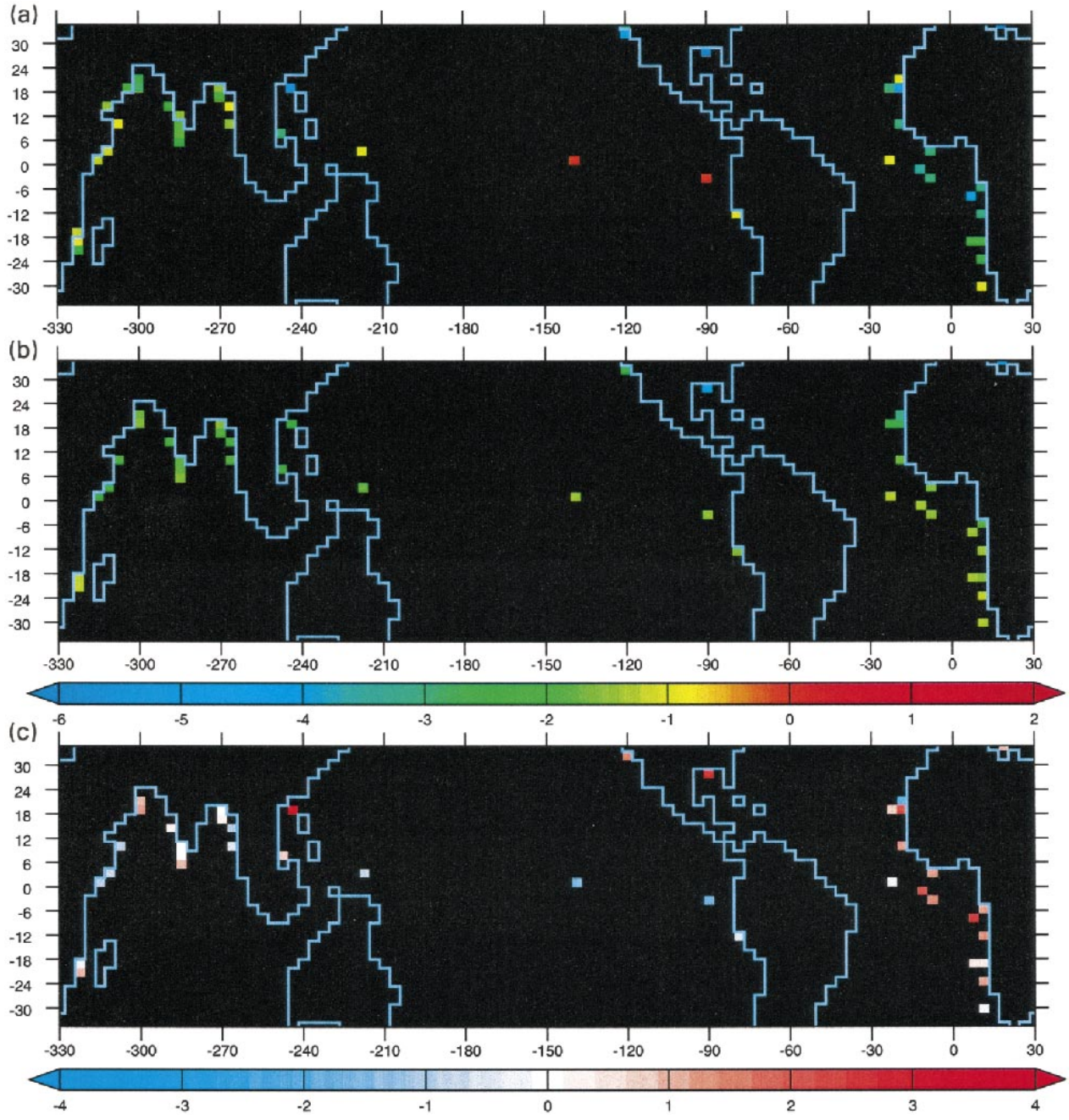

FIG. 13. Same as Fig. 9 except paleotemperature data are SST reconstructions based on alkenones (Rosell-Melé et al. 1998).

an intermediate level of cooling in eastern equatorial South America. Given the near uniformity of the noble gas temperature anomalies, the model–paleodata discrepancies range from −1 to −3 K in southern North America to +2 K at the South American grid point and as much as +3 K in southern Africa. The spatial averages for the 35°N to 35°S region, which should be interpreted with great caution due to paucity of available sites, mask these systematic variations. The noble gas anomalies average −5.1 K as compared with the simulated spatially averaged land surface temperature change based on the same locations of −4.0 K, yielding a model–paleodata discrepancy of +1.1 K.

e. Pollen and other terrestrial indicators

Pollen data provide evidence of past vegetation, which in some circumstances can be interpreted as changes in surface climate through the use of an ''inverse modeling'' approach (Bartlein et al. 1998). Esti-

TABLE 4. Grid point values of LGM surface air temperature anomalies (K) reconstructed from noble gases and simulated by the climate model. Because these quantities are presented on the climate model grid, individual entries may include more than one paleotemperature reconstruction.

Lat (°)	Long (°)	Noble gas ΔT	Simulated ΔT	Model–paleodata discrepancy
−32.4	26.3	−5.5	−1.9	+3.6
−23.5	18.8	−5.3	−2.1	+3.2
−7.8	−41.3	−5.4	−2.8	+2.6
28.0	−97.5	−5.2	−5.3	−0.1
32.4	−82.5	−4.0	−6.8	−2.8

mates of changes in surface air temperature made in this general way have been compiled under the auspices of PMIP (Farrera et al. 1999), and Pinot et al. (1999) have used these estimates in their model–data comparison. These paleotemperature anomalies, which represent the change in the temperature of the coldest month, are used as input to the procedure described at the beginning of this section. The pollen-derived paleotemperature anomalies are compared to the simulated changes in the surface air temperature of the coldest month taken from the LGM integration.

In the domain extending from 35°N to 35°S, the pollen-derived anomalies vary widely, ranging between −1 and −15 K (Fig. 14a). Some spatial patterns are evident from these paleotemperature reconstructions. The cooling is very large in southeastern North America and southeastern Asia, with anomalies of between −6 and −15 K. The cooling is somewhat smaller elsewhere, with most sites south of 20°N indicating anomalies between −4 and −8 K. Anomalies between −4 and −6 K are typical of most locations in the deep Tropics, with some smaller changes in the Australasian sector.

The simulated changes in surface air temperature (Fig. 14b) have some common features with the pollen-derived estimates, such as a relatively large cooling in southeastern North America and a more modest cooling south of 20°N. The simulated North American cooling south of 20°N is only about half of that estimated from pollen evidence. Thus positive model–paleodata discrepancies dominate the area south of 20°N (Fig. 14c), with smaller discrepancies in the Eastern Hemisphere and larger ones in the Americas.

When averaged over the region from 35°N to 35°S, an anomaly of −5.5 K is reconstructed from the Farrera et al. (1999) database, as compared with a spatial mean anomaly of −2.4 K computed from the output from the LGM integration sampled at the same points. Even more so than in the case of the noble gas paleotemperatures, the simulated cooling is substantially smaller than suggested by the paleodata.

Farrera et al. (1999) have recently analyzed these temperature reconstructions and found the magnitude of the LGM cooling to depend on elevation, with greater cooling from high-altitude sites. Since the topography used in the A–MLO model is rather smooth, in many cases the pollen-derived paleotemperature estimates come from substantially higher elevations than the corresponding model output, potentially adding to the discrepancy between the simulated and reconstructed cooling. Farrera et al. (1999) adjusted for elevation differences by using only sites below 1500 m and performing an empirical adjustment based on a linear regression between LGM temperature anomaly and elevation. As a result of this adjustment, the pollen-derived estimates of tropical cooling are reduced in magnitude, thus bring them in closer agreement with the model. Nonetheless, the pollen-derived estimates remain larger at most locations, especially in Central and South America.

f. Mountain snowlines

Additional evidence regarding the thermal climate of the LGM is available in the form of moraines left behind after the downward expansion of mountain glaciers during that period. From these landforms, glacial geologists can reconstruct the position of the equilibrium line, or the level above which snow accumulation exceeds ablation. Since there is a close correspondence between the equilibrium line and the annual mean freezing level, excursions in equilibrium line elevation are often interpreted as providing information about low latitude temperature changes at high elevations? S.C. Porter (1998, personal communication) has compiled a dataset containing the changes in equilibrium line elevation during the LGM. Because they are expressed relative to modern sea level, these changes represent the sum of change of equilibrium line elevation relative to contemporaneous sea level and the ~105 m change in sea level between the LGM and today. The procedure used to compare these paleodata with the A–MLO simulation is the same as has been used throughout this section, except that the estimated snow line depressions are compared with simulated changes in the altitude of freezing level taken from the LGM integration. The magnitude of the simulated changes has been increased by 105 m to adjust for the change in sea level.

The snow line depression values range from 650 to 1180 m, and show no distinct pattern (Table 5). The mean value of approximately 900 m would correspond to a temperature change of ~5 K at the elevation of the snow line if the lapse rate is assumed to be moist adiabatic, which is a good approximation for much of the Tropics. The changes in freezing level simulated by the model are more uniform and substantially smaller than the snow line changes, ranging from 425 to 580 m, with a mean of 515 m. This mean value is similar to that obtained by giving the tropical boundary layer model of Betts and Ridgway (1992) the mean SST and sea level pressure changes from the LGM simulation. The model–paleodata discrepancies, here computed as the difference between the simulated change in freezing level elevation and the estimated change in equilibrium

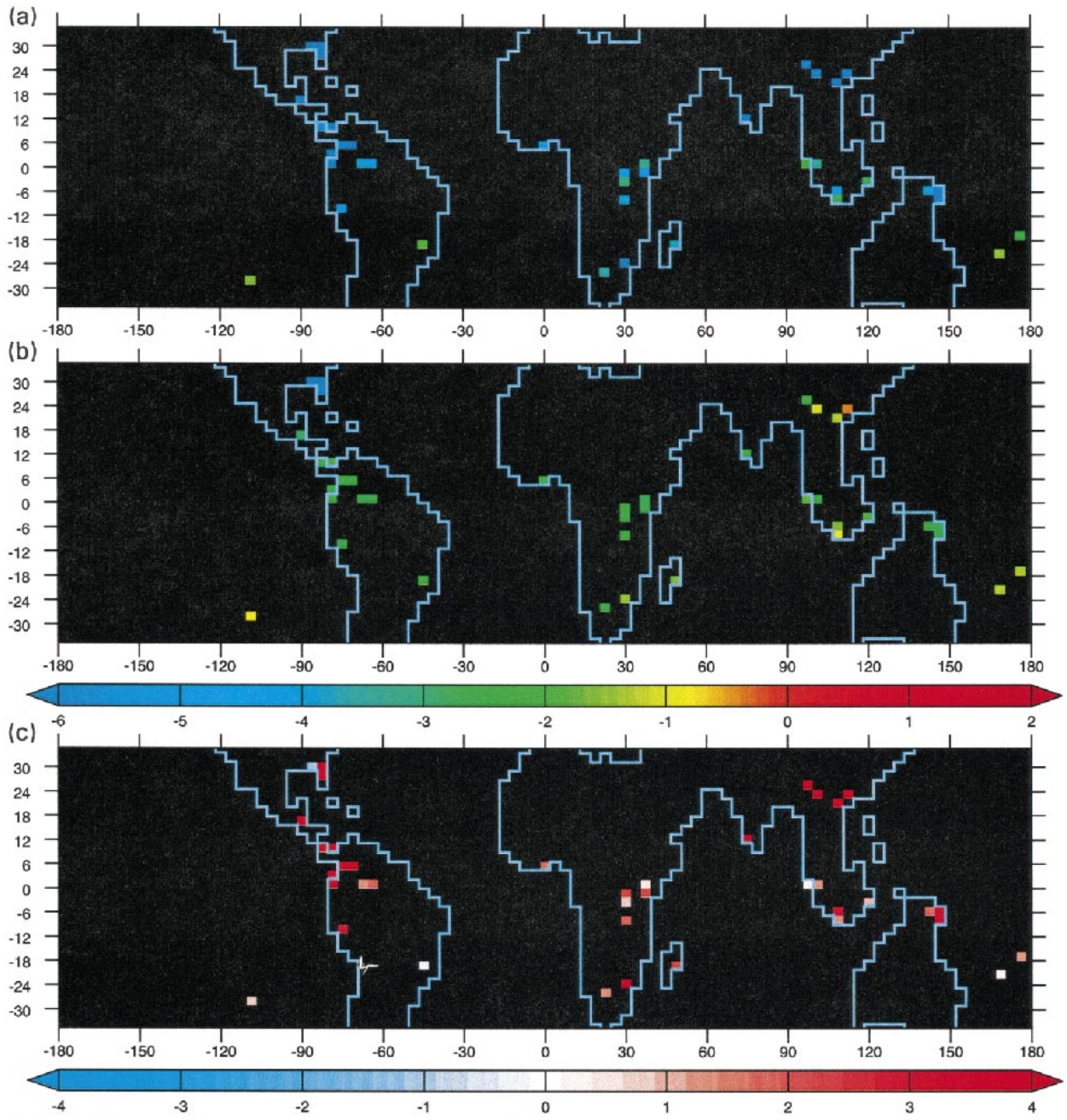

FIG. 14. Same as Fig. 9 except paleotemperature data are annual mean temperature based on pollen and other terrestrial indicators (Farrera et al. 1999) and model output is difference in surface air temperature of coldest month.

line elevation, are primarily in excess of 350 m. Smaller discrepancies are located at a few locations, all of which are located within a few degrees of the equator, but there is insufficient evidence to determine if this represents a spatial pattern of physical importance.

Interpreting the snow line depression data involves considerable uncertainty. As noted by Farrera et al. (1999), the elevation dependence of the temperature near the ground (the ''slope lapse rate'') is not necessarily the same as the lapse rate in the free atmosphere. Any difference between these two lapse rates would complicate a comparison between changes in equilibrium line altitude and freezing level. In a simulation with a regional climate model, Giorgi et al. (1997) found that the warming over Europe associated with a doubling of atmospheric CO_2 increased with elevation, raising the possibility that an LGM climate simulation using a model with much higher resolution may be able to generate a larger cooling at high elevation sites in the Tropics. Although a quantitative resolution of this issue

TABLE 5. Grid point values of reconstructed LGM changes in equilibrium line altitudes (ΔELA, in m) and changes in freezing level simulated by the climate model. Because these quantities are presented on the climate model grid, individual entries may include more than one equilibrium line reconstruction.

Lat (°)	Long (°)	ΔELA	Simulated Δfreezing level	Model–paleodata discrepancy
1.1	30.0	−650	−577	+73
−5.6	37.5	−900	−559	+341
28.0	86.3	−930	−425	+505
−5.6	146.2	−940	−526	+414
19.0	−97.5	−1000	−582	+418
7.8	−71.3	−910	−532	+378
5.6	−75.0	−1010	−539	+471
−1.1	−78.8	−820	−523	+297
−7.8	−75.0	−660	−478	+182
−16.8	−67.5	−930	−462	+468
−21.2	−67.5	−930	−481	+449
−23.5	−67.5	−1180	−487	+693

remains out of reach, available evidence suggests that some caution is advised in interpreting the mountain snow line evidence in terms of temperature change.

g. Isotopes in corals

Ratios of strontium to calcium in the growth bands of living corals have been found to vary in concert with the seasonal cycle of temperature of the water in which the corals live (Beck et al. 1992). This relationship provides the basis for estimating the history of SST changes by determining the strontium–calcium ratio in fossil corals. The development of better analytical methods for determining this ratio has facilitated paleoclimatic reconstructions that indicate changes in low-latitude glacial SSTs that are considerably larger than those derived from species abundances or alkenones.

The spatial coverage of paleotemperature estimates based on this method is very limited at present. Beck et al. (1992) estimated that SSTs at Vanuatu in the western South Pacific were as much as 5 K colder than present during the deglaciation, suggesting that glacial temperatures may have been at least as low. Guilderson et al. (1994) used a sample of glacial age from Barbados and estimated a 4–5-K LGM cooling at that location. At each of these locations, the cooling simulated in the LGM integration is considerably smaller. In the vicinity of Barbados the simulated cooling is 2–2.5 K, while a cooling of 1–1.5 K is indicated near Vanuatu.

8. Implications for climate model sensitivity

The comparisons discussed in the previous section are relevant to the ongoing debate about the sensitivity of tropical temperatures to radiative forcing, both in the context of past climates (Crowley 1991, 1993) and in projections of future climate change (Lindzen 1994), as they provide an avenue for assessing whether the response of the climate model is realistic. Such an assessment is complicated by the substantial uncertainties inherent in the use of temperature reconstructions based on paleoclimatic proxies. Nevertheless, there is considerable value in exploring the implications of the model–paleodata comparisons for broader issues such as the mechanisms by which tropical temperatures are controlled and reliability of model-derived estimates of tropical climate sensitivity.

a. Synthesis of proxy evidence for LGM temperature changes

The contrasting estimates of the large-scale LGM temperature change coming from different lines of evidence make it difficult to assemble a coherent picture of tropical temperature changes based on the paleoclimatic record. Species abundances of marine microorganisms, using both transfer function (i.e., CLIMAP) and modern analog methods, and alkenones indicate relatively modest cooling (1–2.5 K), while noble gases, pollen, snowlines, and corals yield larger cooling estimates (~5 K).

Explanations can be offered for the apparent conflict among these different lines of evidence. For example, the differences among these proxy estimates could be characterized as representing a difference between oceanic and continental response. Indeed, all of the proxies that suggest modest cooling come from the oceans, while all of the continental proxies are indicative of larger cooling. Paleotemperatures based on the isotopic composition of corals have complicated this simple interpretation, yielding estimates of glacial cooling that are quite comparable in magnitude to the estimates of terrestrial temperature change. In a similar vein, both the coral evidence and the noble gas paleothermometer would appear to contradict the hypothesis that the large glacial cooling occurred only at higher elevations.

Although a satisfactory, physically consistent reconciliation of all of the available paleotemperature evidence does not appear possible at this time, it may be useful to construct some plausible scenarios of LGM temperature change to provide some context for the model results. The specific scenarios that follow are not intended to be the only possible interpretations of the paleoclimatic record; however, it is likely that the actual LGM climate fell somewhere within their range.

One possible interpretation is to accept the evidence from the species abundances of marine microorganisms (i.e., the CLIMAP and modern analog reconstructions) and alkenones as representative of both terrestrial and oceanic conditions. Neglecting regional variations, this scenario would imply an LGM cooling of 1–2.5 K. The surface air temperature reduction in the LGM simulation of 2.0 K is within this range, suggesting that the low-latitude temperature sensitivity simulated by the climate model would be quite realistic under this scenario.

Another possibility is to assume that the paleotem-

peratures reconstructed from noble gases in aquifers, pollen, snow line depressions, and isotopes in corals are correct and indicative of both continental and oceanic conditions. Neglecting regional variations once again, this would imply a cooling of ~5 K, substantially in excess of the temperature changes simulated by the climate model.

A third scenario can be constructed by accepting the species abundance and alkenone estimates of modest changes in ocean temperature while also accepting the noble gas, pollen, and snow line depression evidence for large temperature changes over the continents. In essence, paleotemperatures derived from all the lines of evidence are accepted with the exception of those based on the isotopic composition of corals. Under this scenario, a substantial contrast would exist between the terrestrial and oceanic cooling, with larger cooling over land. Indeed, the simulated cooling is larger over the continents (ΔSAT = −2.7 K) as compared to the oceans (ΔSAT = −1.7 K). As discussed in section 5, the lowering of sea level at the LGM and the difference in evaporative damping between land and sea contribute in nearly equal portions to the simulated contrast in ΔSAT. Thus the simulated temperature sensitivity under this scenario would be quite realistic over the oceans but substantially underestimated for land.

Based on the comparisons described in the preceding subsection, the tropical sensitivity of the model is most likely similar to, or perhaps smaller than, that of the real climate system. The probability that the model substantially exaggerates the sensitivity would appear to be rather low, and would require both the acceptance of a low sensitivity interpretation of the paleoclimatic evidence for oceans and continents, as well as the existence of important negative radiative forcing from sources not included in the LGM simulation.

b. Other climate forcings

The experimental design used in this study does not account for all possible sources of LGM radiative forcing. Methane and nitrous oxide were less abundant in the glacial atmosphere, but reductions in these gases were not included in the LGM integration. As discussed in section 3, their contribution would only add about 16% to the total radiative forcing of −4.2 W m^{-2}. In addition, changes in vegetation and atmospheric dust loading were not included in the PMIP specifications. Both vegetation and dust have been hypothesized as sources of negative radiative forcing.

The climatic importance of LGM vegetation changes has been examined in previous modeling studies. Broccoli and Manabe (1987) used an earlier version of an A–MLO model to estimate the contribution of vegetation changes to the LGM climate, using the CLIMAP (CLIMAP Project Members 1981) vegetation reconstruction for the LGM. They found that vegetation changes contributed an additional ~25% to the low-latitude cooling produced by ice sheet and CO_2 forcing combined. More recently, Crowley and Baum (1997) modeled the ice age vegetation effect using an independently derived set of LGM vegetation changes. In their simulation, low-latitude continental temperatures underwent a regionally dependent change of ±1 K; however, the overall vegetation-induced low-latitude temperature change may have been muted by the use of prescribed SSTs. The results of these two studies suggest that vegetation changes may have local or regional importance, but are not likely to represent a large climate forcing on the global scale.

Because of ice core evidence for increased deposition during glacial times, dust has also been regarded as a potential source of negative radiative forcing. Harvey (1988) used an energy balance model driven by relatively large estimates of the global radiative forcing from dust (−2.6 W m^{-2}) to simulate a cooling of 1.7 K for the deep Tropics as a result of dust alone. Other estimates of ice age aerosol forcing are approximately −1 W m^{-2} (Hoffert and Covey 1992; Hansen et al. 1993), which would augment the radiative forcing used in the LGM simulation by ~25%. The most recent work suggests that the effects of dust may be more complicated because of the interplay between radiative cooling effects at the surface and heating effects in the troposphere due to absorption of shortwave radiation (Tegen et al. 1996; Overpeck et al. 1996). Thus large uncertainties remain in estimating the climatic effects of dust, making even the sign of the resulting surface air temperature response subject to some question.

c. Comparison with sensitivity to CO_2 doubling

One can compare the sensitivity of the current model in response to LGM forcing to its sensitivity to a doubling of atmospheric CO_2. An additional integration of the A–MLO model, in which the atmospheric CO_2 concentration is twice that of the modern integration, is used for this purpose. A global sensitivity parameter λ is defined, where $\lambda = \Delta T/\Delta Q$, ΔT is the global mean surface air temperature response, and ΔQ is the global mean radiative forcing (Cubasch and Cess 1992). Using values of ΔT and ΔQ from the LGM integration yields a global sensitivity parameter of 0.95, which is nearly 25% larger than the value of 0.77 computed from the $2 \times CO_2$ integration (Table 6). Whether this difference is meaningful is unclear, since the ΔT value from the LGM integration includes the temperature changes that arise at those locations in which the continental ice sheets of the LGM have a different elevation than the same grid points in the modern integration. Using a value averaged over only those grid points that are ice free in the LGM integration yields an adjusted sensitivity parameter of 0.75, which is very similar to that of the $2 \times CO_2$ run.

A tropical sensitivity parameter λ_{tropics} can be defined, where $\lambda_{\text{tropics}} = \Delta T_{\text{tropics}}/\Delta Q$, ΔQ is defined as above, and

TABLE 6. Climate sensitivity parameters for the LGM and 2 × CO_2 integrations. (Symbols are defined in text.)

	ΔT	ΔQ	λ	$\Delta T_{tropics}$	$\lambda_{tropics}$
LGM	−4.0	−4.20	0.95	−2.0	0.48
2 × CO_2	3.2	4.15	0.77	2.3	0.55
LGM (ice points excluded)	−3.2	—	0.75	—	—

$\Delta T_{tropics}$ is the mean surface air temperature change from 30°N to 30°S. The values of $\lambda_{tropics}$ are 0.48 and 0.55 for the LGM and 2 × CO_2 integrations, respectively. In both cases $\lambda_{tropics} < \lambda$, indicative of the ''polar amplification'' of the temperature response.

This relationship between high- and low-latitude thermal response is model dependent (Rind 1987), as has been noted in comparisons of doubled CO_2 simulations from different climate models. The recent LGM simulation by Webb et al. (1997) demonstrates that it is possible to simulate a tropical cooling (−5.7 K) that is nearly three times as large as that of the model used in this study while employing virtually the same forcing. The global sensitivity of their model to LGM forcing, however is only twice as large (−8 K), indicating a different degree of polar amplification. Although this paper focuses on tropical temperature changes, the contrast with the results of Webb et al. (1997) reinforces the need to consider systematic spatial variations when using paleo-data to evaluate model performance.

The similarity between the LGM and 2 × CO_2 integrations of the values of $\lambda_{tropics}$ and λ (after adjusting for ice sheet elevation changes) suggests that similar feedback mechanisms are operating in both the integrations. This provides some justification for assuming than the assessment of model sensitivity for the LGM case may be applicable to anthropogenic trace gas forcing as well, which would imply that there is insufficient evidence from glacial paleoclimates to rule out substantial future changes in low-latitude temperatures.

9. Summary and discussion

This paper examines the sensitivity of tropical temperature to glacial forcing by integrating an A–MLO model with alterations in sea level, continental ice, atmospheric CO_2, and orbital parameters characteristic of the last glacial maximum. The temperature changes simulated in this integration are compared with paleoclimatic reconstructions of the glacial climate, with the focus on low latitudes. The primary findings are summarized below.

- The global radiative forcing of −4.20 W m^{-2} associated with the changes in sea level, continental ice, atmospheric CO_2, and orbital parameters leads to a decrease in global mean surface air temperature of 4.0 K, with the largest cooling in the Northern Hemisphere extratropics.
- In the Tropics (30°N–30°S), the change in surface air temperature is −2.0 K, but with considerable spatial variability that results from land–sea contrast, advective effects, changes in soil moisture, and the interhemispheric asymmetry of radiative forcing.
- Tropical cooling over land averages 2.7 K, as compared with a 1.7 K cooling over the tropical oceans. Approximately half this difference is a result of the 105-m lowering of sea level, while differences in the partitioning of net radiation between latent and sensible heating account for most of the remainder.
- The decrease in top-of-atmosphere longwave emission associated with this tropical cooling is balanced primarily by a combination of increased reflection of shortwave radiation by clouds and an increase in atmospheric heat transport to the extratropics.
- The mean low-latitude cooling simulated by the model is comparable to that reconstructed from alkenones or species abundances of planktonic microfossils, but smaller than the cooling inferred from noble gas, pollen, snowline depression, or coral evidence.
- Based on these comparisons with paleodata, it is unlikely that the climate model exaggerates the actual sensitivity of tropical climate to glacial forcing, even when the uncertainties in both forcing and reconstructed climate are taken into account.

The last of these findings has implications for possible future changes in climate associated with anthropogenic greenhouse gases. When forced by a doubling of atmospheric CO_2, the A–MLO model used in this study simulates a global warming of 3.2 K. As in the case of glacial forcing, the warming in the Tropics is somewhat smaller, averaging 2.3 K. Since the comparisons with paleodata imply that the actual sensitivity of tropical temperature is unlikely to be substantially smaller than this model, one might expect a significant rise in tropical temperatures in response to projected increases in greenhouse gas forcing. Only an extreme asymmetry in the feedback mechanisms associated with warming and cooling would allow tropical temperature to be insensitive to such forcing. Present climate models provide no evidence for such extreme asymmetry.

The tropical sensitivity exhibited by the A–MLO model used in this study should not be extrapolated to be characteristic of other climate models. A comparison of glacial simulations with models of this type undertaken by PMIP indicates a wide range of tropical sensitivities, which are presumed to arise from the many differences in detail in the construction of these models, including the representation of such physical processes as the relationship between clouds and climate (Pinot et al. 1999). At present, the differences in the magnitude

of tropical cooling reconstructed from the various paleoclimatic proxies preclude a determination of which models are most realistic in their simulation of the tropical sensitivity to glacial forcing.

An important element that is absent from the simulation discussed in this study is the interaction with ocean dynamics. A number of mechanisms have been proposed in which such interactions might play an important role in determining the sensitivity of tropical temperatures (Clement et al. 1996; Clement and Seager 1998; Seager and Murtugudde 1997; Sun and Liu 1996; Gu and Philander 1997; Bush and Philander 1998). The use of coupled atmosphere–ocean general circulation models is required to quantitatively evaluate the importance of such mechanisms relative to the other factors that influence tropical climate sensitivity.

Recently, several groups have simulated the glacial climate using models that include a representation of ocean dynamics. Ganopolski et al. (1998) used a statistical–dynamical model of the atmosphere coupled to a 2.5-dimensional ocean GCM. By integrating their model until it was fully equilibrated to the glacial forcing, they simulated a global cooling of just over 6 K, accompanied by changes in ocean circulation and heat transport. Bush and Philander (1998) simulated the glacial climate by making a relatively short integration (15 yr, including spinup) with a three-dimensional atmospheric GCM coupled with a three-dimensional ocean model. Tropical temperatures in their model cooled by as much as 6 K, which they attributed to the feedback between trade wind intensity and upwelling strength and the equatorward flow of cold water in the thermocline. Weaver et al. (1998) coupled an energy–moisture balance model of the atmosphere to a three-dimensional ocean GCM. Their most interesting finding was a dependency of the magnitude of the change in thermohaline overturning on the intensity of this circulation in the control case.

All three of these recent studies can be seen as intermediate steps toward the goal of completing a fully equilibrated simulation of the ice age climate using a three-dimensional atmospheric GCM coupled with a three-dimensional ocean model. Such a simulation, if technically feasible, would represent a very significant advance in climate modeling. Problems with initialization, climate drift (i.e., the need for flux adjustments), and computational expense currently preclude simulations of this kind. Different research groups have chosen different ways to circumvent these technical obstacles. Ganopolski et al. (1998) used very coarse resolution of atmospheric processes with the effects of transient eddies parameterized rather than explicitly included, and represented the ocean as three zonally averaged basins connected at their southern ends. Bush and Philander (1998) used a more comprehensive model, but made only a short integration rather than allowing for the coupled system to be fully equilibrated. By using an energy–moisture balance atmospheric component, Weaver et al. (1998) greatly simplified the atmospheric component of their model.

In the present study, the use of a slab ocean also constitutes a simplification of the processes operating in the actual climate system. This strategy is consistent with the aim of studying the atmospheric mechanisms influencing climate sensitivity. As with the studies discussed previously, this approach is reasonable provided that the results are interpreted with appropriate caution. In this case, such caution includes the understanding that these simulations exclude interactions that involve ocean dynamics. Ultimately, our understanding of glacial climate will be best served by the simulation of an equilibrium glacial climate using a three-dimensional atmospheric GCM coupled to a three-dimensional ocean GCM. A simulation of this kind remains a high-priority target for future research.

Acknowledgments. I am indebted to S. Manabe for his continuing support and encouragement regarding this and other projects. R. Avissar, T. Crowley, L. Donner, C. Jackson, I. Held, J. Mahlman, S. Manabe, J. Miller, D. Robinson, and B. Soden provided helpful comments on this paper, as did an anonymous reviewer. S. Porter, R. Schneider, and M. Stute kindly provided compilations of paleodata. C. Raphael provided her assistance in preparing the figures for electronic submission.

REFERENCES

Anderson, D. M., W. L. Prell, and N. J. Barratt, 1989: Estimates of sea surface temperature in the Coral Sea at the last glacial maximum. *Paleoceanography,* **4,** 615–627.

Bard, E., B. Hamelin, R. G. Fairbanks, and A. Zindler, 1990: Calibration of the ^{14}C timescale over the past 30,000 years using mass spectrometric U-Th ages from Barbados corals. *Nature,* **345,** 405–410.

Barnola, J. M., D. Raynaud, Y. S. Korotkevich, and C. Lorius, 1987: Vostok ice core provides 160,000-year record of atmospheric CO_2. *Nature,* **329,** 408–414.

Bartlein, P. J., and Coauthors, 1998: Paleoclimate simulations for North America over the past 21,000 years: Features of the simulated climate and comparisons with paleoenvironmental data. *Quat. Sci. Rev.,* **17,** 549–585.

Beck, J. W., R. L. Edwards, E. Ito, F. W. Taylor, J. Recy, F. Rougerie, P. Joannot, and C. Henin, 1992: Sea-surface temperature from coral skeletal strontium–calcium ratios. *Science,* **257,** 644–647.

Berger, A. L., 1978: Long-term variations of daily insolation and quaternary climate changes. *J. Atmos. Sci.,* **35,** 2362–2367.

Betts, A. K., and W. Ridgway, 1992: Tropical boundary layer equilibrium in the last ice age. *J. Geophys. Res.,* **97,** 2529–2534.

Bourke, W., 1972: An efficient, one-level, primitive-equations spectral model. *Mon. Wea. Rev.,* **100,** 683–689.

Brassell, S. C., G. Eglinton, I. T. Marlowe, U. Pflaumann, and M. Sarnthein, 1986: Molecular stratigraphy: A new tool for climatic assessment. *Nature,* **320,** 129–133.

Broccoli, A. J., and S. Manabe, 1987: The influence of continental ice, atmospheric CO_2, and land albedo on the climate of the last glacial maximum. *Climate Dyn.,* **1,** 87–99.

——, and ——, 1992: The effects of orography on midlatitude Northern Hemisphere dry climates. *J. Climate,* **5,** 1181–1201.

——, and E. P. Marciniak, 1996: Comparing simulated glacial climate and paleodata: A reexamination. *Paleoceanography,* **11,** 3–14.

Broecker, W. S., 1995: *The Glacial World According to Wally*. Eldigio Press, 318 pp.

Bush, A. B. G., and S. G. H. Philander, 1998: The role of ocean–atmosphere interactions in tropical cooling during the last glacial maximum. *Science,* **279,** 1341–1344.

Chen, C.-T., and V. Ramaswamy, 1996: Sensitivity of simulated global climate to perturbations in low cloud microphysical properties. Part II: Spatially localized perturbations. *J. Climate,* **9,** 2788–2801.

Clark, J. F., M. Stute, P. Schlosser, S. Drenkard, and G. Bonani, 1997: A tracer study of the Floridan Aquifer in southeastern Georgia: Implications for groundwater flow and paleoclimate. *Water Resour. Res.,* **33,** 281–289.

Clement, A., and R. Seager, 1998: Climate and the tropical oceans. *J. Climate,* **12,** 3383–3401.

——, ——, M. A. Cane, and S. E. Zebiak, 1996: An ocean dynamical thermostat. *J. Climate,* **9,** 2190–2196.

CLIMAP Project Members, 1976: The surface of the ice-age earth. *Science,* **191,** 1131–1137.

——, 1981: Seasonal reconstructions of the earth's surface at the last glacial maximum. Geological Society of America Map and Chart Series MC-36, 18 pp. [Available online at http://geosociety.org.]

Crowley, T. J., 1991: Past CO_2 changes and tropical sea surface temperatures. *Paleoceanography,* **6,** 387–394.

——, 1993: Geological assessment of the greenhouse effect. *Bull. Amer. Meteor. Soc.,* **74,** 2363–2373.

——, and S. K. Baum, 1997: Effect of vegetation on an ice-age climate model simulation. *J. Geophys. Res.,* **102,** 16 463–16 480.

Cubasch, U., and R. D. Cess, 1990: Processes and modelling. *Climate Change: The IPCC Scientific Assessment,* J. T. Houghton, G. J. Jenkins, and J. J. Ephraums, Eds., Cambridge University Press, 69–91.

Farrera, I., and Coauthors, 1999: Tropical climates at the last glacial maximum: A new synthesis of terrestrial palaeoclimate data. I. Vegetation, lake-levels and geochemistry. *Climate Dyn.,* **15,** 823–856.

Flato, G. M., and W. D. Hibler III, 1992: Modeling pack ice as a cavitating fluid. *J. Phys. Oceanogr.,* **22,** 626–651.

Ganopolski, A., S. Rahmstorf, V. Petoukhov, and M. Claussen, 1998: Simulation of modern and glacial climate with a coupled model of intermediate complexity. *Nature,* **391,** 351–356.

Giorgi, F., J. W. Hurrell, M. R. Marinucci, and M. Beniston, 1997: Elevation dependence of the surface climate change signal: A model study. *J. Climate,* **10,** 288–296.

Gordon, C. T., and W. F. Stern, 1982: A description of the GFDL global spectral model. *Mon. Wea. Rev.,* **110,** 625–644.

Gu, D., and S. G. H. Philander, 1997: Interdecadal climate fluctuations that depend on exchanges between the tropics and extratropics. *Science,* **275,** 805–807.

Guilderson, T. P., R. G. Fairbanks, and J. L. Rubenstone, 1994: Tropical temperature variations since 20,000 years ago: Modulating interhemispheric temperature change. *Science,* **263,** 663–665.

Hansen, J., A. Lacis, D. Rind, G. Russell, P. Stone, I. Fung, R. Ruedy, and J. Lerner, 1984: Climate sensitivity: Analysis of feedback mechanisms. *Climate Processes and Climate Sensitivity,* J. E. Hansen and T. Takahashi, Eds., Amer. Geophys. Union, 130–163.

——, ——, R. Ruedy, M. Sato, and H. Wilson, 1993: How sensitive is the world's climate? *Natl. Geogr. Res. Explor.,* **9,** 142–158.

Harvey, L. D. D., 1988: Climatic impact of ice-age aerosols. *Nature,* **334,** 333–335.

Heaton, T. H. E., A. S. Talma, and J. C. Vogel, 1986: Dissolved gas paleotemperatures and $\delta^{18}O$ variations derived from groundwater near Uitenhage, South Africa. *Quat. Res.,* **25,** 79–88.

Hewitt, C. D., and J. F. B. Mitchell, 1997: Radiative forcing and response of a GCM to ice age boundary conditions: Cloud feedback and climate sensitivity. *Climate Dyn.,* **13,** 821–834.

Hoffert, M. I., and C. Covey, 1992: Deriving global climate sensitivity from paleoclimate reconstructions. *Nature,* **360,** 573–576.

Joussaume, S., and K. E. Taylor, 1995: Status of the Paleoclimate Modeling Intercomparison Project (PMIP). *Proceedings of the First International AMIP Scientific Conference,* W. L. Gates, Ed., World Meteorological Organization, 425–430.

Lacis, A. A., and J. E. Hansen, 1974: A parameterization for the absorption of solar radiation in the earth's atmosphere. *J. Atmos. Sci.,* **31,** 118–133.

Lee, K. E., and N. C. Slowey, 1999: Cool surface waters of the subtropical North Pacific Ocean during the last glacial. *Nature,* **397,** 512–514.

Lindberg, C., and A. J. Broccoli, 1996: Representation of topography in spectral climate models and its effect on simulated precipitation. *J. Climate,* **9,** 2641–2659.

Lindzen, R. S., 1994: Climate dynamics and global change. *Annu. Rev. Fluid Mech.,* **26,** 353–378.

Manabe, S., 1969: Climate and the ocean circulation. I. The atmospheric circulation and the hydrology of the earth's surface. *Mon. Wea. Rev.,* **97,** 739–774.

——, and R. J. Stouffer, 1980: Sensitivity of a global climate model to an increase of CO_2 concentration in the atmosphere. *J. Geophys. Res.,* **85,** 5529–5554.

——, and A. J. Broccoli, 1985a: The influence of continental ice sheets on the climate of an ice age. *J. Geophys. Res.,* **90,** 2167–2190.

——, and ——, 1985b: A comparison of climate model sensitivity with data from the last glacial maximum. *J. Atmos. Sci.,* **42,** 2643–2651.

——, and R. J. Stouffer, 1996: Low-frequency variability of surface air temperature in a 1000-year integration of a coupled atmosphere–ocean–land surface model. *J. Climate,* **9,** 376–393.

Overpeck, J., D. Rind, A. Lacis, and R. Healy, 1996: Possible role of dust-induced regional warming in abrupt climate change during the last glacial period. *Nature,* **384,** 447–449.

Peltier, W. R., 1994: Ice age paleotopography. *Science,* **265,** 195–201.

Pinot, S., G. Ramstein, S. P. Harrison, I. C. Prentice, J. Guiot, M. Stute, S. Joussaume, and PMIP Participating Groups, 1999: Tropical paleoclimates at the Last Glacial Maximum: Comparison of Paleoclimate Modeling Intercomparison Project (PMIP) simulations and paleodata. *Climate Dyn.,* **15,** 857–874.

Prell, W. L., 1985: The stability of low-latitude sea-surface temperatures: An evaluation of the CLIMAP reconstruction with emphasis on the positive SST anomalies. U.S. Dept. of Energy Rep. DOE/ER/60167, 53 pp. [NTIS DE8501619a.]

Ramaswamy, V., and C.-T. Chen, 1997: Linear additivity of climate response for combined albedo and greenhouse perturbations. *Geophys. Res. Lett.,* **24,** 567–570.

Rind, D., 1987: Doubled CO_2 climate: Impact of the sea surface temperature gradient. *J. Atmos. Sci.,* **44,** 3235–3268.

——, and D. Peteet, 1985: Terrestial conditions at the last glacial maximum and CLIMAP sea surface temperature estimates: Are they consistent? *Quat. Res.,* **24,** 1–22.

Rosell-Melé, A., E. Bard, K.-C. Emeis, P. Farrimond, J. Grimalt, P. J. Mueller, and R. R. Schneider, 1998: TEMPUS: A new generation of sea surface temperature maps. *Eos, Trans. Amer. Geophys. Union,* **79,** 393–394.

Seager, R., and R. Murtugudde, 1997: Ocean dynamics, thermocline adjustment, and regulation of tropical SST. *J. Climate,* **10,** 521–534.

Shine, K. P., R. G. Derwent, D. J. Wuebbles, and J.-J. Morcrette, 1990: Radiative forcing of climate. *Climate Change: The IPCC Scientific Assessment,* J. T. Houghton, G. J. Jenkins, and J. J. Ephraums, Eds., Cambridge University Press, 41–68.

——, Y. Fouquart, V. Ramaswamy, S. Solomon, and J. Srinivasan, 1994: Radiative forcing. *Climate Change 1994: Radiative Forcing of Climate Change and An Evaluation of the IPCC IS92 Emission Scenarios,* J. T. Houghton et al., Eds., Cambridge University Press, 163–203.

Stone, H. M., and S. Manabe, 1968: Comparison among various numerical models designed for computing infrared cooling. *Mon. Wea. Rev.,* **96,** 735–741.

Stute, M., and P. Schlosser, 1993: Principles and applications of the noble gas paleothermometer. *Climate Change in Continental Isotopic Records*, P. K. Swart et al., Eds., Amer. Geophys. Union, 89–99.

——, ——, J. F. Clark, and W. S. Broecker, 1992: Paleotemperatures in the southwestern United States derived from noble gas measurements in groundwater. *Science*, **256,** 1000–1003.

——, M. Forster, H. Frischkorn, A. Serejo, J. F. Clark, P. Schlosser, W. S. Broecker, and G. Bonani, 1995a: Cooling of tropical Brazil (5°C) during the last glacial maximum. *Science*, **269,** 379–383.

——, P. Schlosser, A. S. Talma, A. Herczeg, and A. Love, 1995b: Uniform cooling of the low latitudinal continents during the last glacial maximum. *Eos, Trans. Amer. Geophys. Union*, **76** (Suppl.), F296.

Sun, D.-Z., and Z. Liu, 1996: Dynamic ocean–atmosphere coupling: A thermostat for the tropics. *Science*, **272,** 1148–1150.

Tegen, I., A. A. Lacis, and I. Fung, 1996: The influence on climate forcing of mineral aerosols from disturbed soils. *Nature*, **380,** 419–422.

Weaver, A. J., M. Eby, A. F. Fanning, and E. C. Wiebe, 1998: Simulated influence of carbon dioxide, orbital forcing and ice sheets on the climate of the Last Glacial Maximum. *Nature*, **394,** 847–853.

Webb, R. S., D. H. Rind, S. J. Lehman, R. J. Healy, and D. Sigman, 1997: Influence of ocean heat transport on the climate of the last glacial maximum. *Nature*, **385,** 695–699.

Webster, P. J., and N. A. Streten, 1978: Late Quaternary ice age climates of tropical Australasia: Interpretations and reconstructions. *Quat. Res.*, **10,** 279–309.

Wetherald, R. T., 1996: Feedback processes in the GFDL R30-14 level general circulation model. *Climate Sensitivity to Radiative Perturbations: Physical Mechanisms and Their Validation*, H. Le Treut, Ed., Springer-Verlag, 251–266.

Wilson, C. A., and J. F. B. Mitchell, 1987: A doubled CO_2 climate sensitivity experiment with a global climate model including a simple ocean. *J. Geophys. Res.*, **92,** 13 315–13 343.